T.R.
GEBZE TECHNICAL UNIVERSITY
INSTITUTE OF NANOTECHNOLOGY

MICROFLUIDIC PREPARATION OF METFORMIN-ENCAPSULATED THERMO-SENSITIVE NANOCOMPOSITE HYDROGEL SYSTEMS FOR TOPICAL VAGINAL APPLICATIONS

MELDA ELMAS
A THESIS SUBMITTED FOR THE
DEGREE OF MASTER OF SCIENCE
NANOSCIENCE AND NANOENGINEERING

GEBZE
2022

T.R.

GEBZE TECHNICAL UNIVERSITY

INSTITUTE OF NANOTECHNOLOGY

MICROFLUIDIC PREPARATION OF METFORMIN-ENCAPSULATED THERMO-SENSITIVE NANOCOMPOSITE HYDROGEL SYSTEMS FOR TOPICAL VAGINAL APPLICATIONS

MELDA ELMAS

A THESIS SUBMITTED FOR THE DEGREE OF

MASTER OF SCIENCE

NANOSCIENCE AND NANOENGINEERING

SUPERVISOR
ASSOC. PROF. DR. İSRAFİL KÜÇÜK

CO-SUPERVISOR
ASST PROF. DR. GÜLENGÜL DUMAN

GEBZE

2022

GEBZE TEKNİK ÜNİVERSİTESİ	**YÜKSEK LİSANS JÜRİ ONAY FORMU**

GTÜ Nanoteknoloji Enstitüsü Yönetim Kurulu'nun …..…/…..…/..…… tarih ve ..……/……..… sayılı kararıyla oluşturulan jüri tarafından …..…/…..…/..…… tarihinde tez savunma sınavı yapılan ……'ın tez çalışması ……Anabilim Dalında YÜKSEK LİSANS tezi olarak kabul edilmiştir.

JÜRİ

ÜYE

(TEZ DANIŞMANI) :

ÜYE :

ÜYE :

ONAY

Gebze Teknik Üniversitesi Nanoteknoloji Enstitüsü Yönetim Kurulu'nun

..…/……/…… tarih ve ……/…..... sayılı kararı.

İMZA/MÜHÜR

SUMMARY

Polycystic ovarian syndrome (PCOS), which is an ovarian syndrome triggered by the deficiency of follicle-stimulating hormone (FSH) levels during ovulation, has attracted great interest because it widely affects many women of reproductive age, approximately between the ages of 14 and 49. Lifestyle changes such as diet and exercise help most patients, but some do not respond to them. Thus, medication is inevitable for some patients with PCOS.

Insulin is directly associated with hormonal irregularities. Therefore, insulin-synthesizing drugs have been suggested for the treatment of PCOS. Metformin is widely used as an oral drug in cases of type II diabetes, but it has been reported to have side effects such as gastrointestinal problems. These problems are related to the oral administration of the drug. Vaginal drug administration is often preferred for hormonal disorders and other diseases due to the highly absorptive nature of the vagina. Research studies have previously examined the effects of metformin in the treatment of PCOS.

The purpose of this research was to produce nanocomposite stimuli-responsive hydrogel platforms for vaginal drug delivery. Nanocomposite hydrogels enable the controlled release of a drug. To confirm the successful incorporation of nanocomposite hydrogels either with or without liposomal nanoparticles, drug release and other characterization methods were designed and applied. In vitro release tests were performed to evaluate the release profiles of the hydrogels and the controlled-release profile of metformin in dissolution medium was accordingly observed. The results demonstrated that liposomal nanoparticles were successfully trapped in the nanocomposite hydrogel. These findings show that the nanocomposite hydrogel platforms prepared in this research are promising for controlled delivery applications.

Key words: Hydrogel, vaginal drug delivery, nanocomposite, controlled-release drug delivery, metformin.

ÖZET

Polikistik over sendromu (PKOS) yumurtlama döneminde folikül uyarıcı hormon (FSH) düzeylerindeki eksikliklerle tetiklenen üreme dönemindeki (14-49 yaş) birçok kadını etkilenmekte olam bir vajinal rahatsızlık olup, bu yönüyle ilgi çeken bir konudur. Her ne kadar düzenli egzersiz ve diyet hastalara yardımcı olsa da, bazı hastalarda etkili bir tedavi yöntemi olarak cevap vermemektedir ve bu hastalarda hormonların dengelenmesi adına ilaç tedavisi uygulanması kaçınılmazdır. İnsülin doğrudan hormonlarla ilişkildir. Bu nedenle FSH hormonun uyarılması adına insülin sentezleyici ilaçlar önerilmektedir. Metformin, tip II diyabet hastaları tarafından yaygın olarak kullanılan oral formda alınmasına bağlı mide bulantisi ve gastrointestinal problemler gibi yan etkileri bulunan bir ilaç olarak bildirilmiştir. Yan etkilerini olmasının temel nedeni ilacın oral yolla verilmesiyle ilişkilidir. Bu sebeple nazal, vajinal, ve transdermal yol gibi alternatif ilaç veriliş yolları geliştirlmektedir. Vaginal ilaç uygulanma yöntemi, vajinanın sahip olduğu yüksek emici özelliğinin sağladığı avantaj sayesinde tercih edilen bir uygulama yöntemidir. Literatürde bazı çalışmalar PKOS için vajinal ilaç uygulamalarını içermektedir. Bu yüksek lisans tez çalışmasında vajinal ilaç taşınım sistemi hedeflenerek, içerisine ilaç ilave edilmiş, dış uyaranlara duyarlı nanokompozit yapıdaki hidrojel platfromlar elde etmek ve elde edilen bu yapıların karakterizasyonu amaçlanmışıtr. Böylece ilaç ilave edilmiş sıcaklığa duyarlı hidrojellerle, vajinal ortamda ilacın kontrollü salınımı sürdürülebilecektir. Hidrojellere lipozomal yapıda veya sadece metformin'in başarılı bir şekilde dahil edilmesini ortaya çıkarmak için ilaç salımı ve karakterizasyon çalışmaları dizayn edilip kullanıldı. In vitro ilaç salım çalışmalarında, metformin'in kontrollü salımına tanık olunulmuştur. Destekleyici nitelikte olan bulgularda dahidrojel platfromlarının içerisindeki lipozomal nanoparçacıkların hidrojel ağında hapsolması gözlemlenmiştir. Bulgularımız, bu geliştirilen nanokompozit hidrojel platfromların seçilen çözünme ortamında kontrollü ilaç salımı açısından umut verici nitelikte olduğunu göstermektedir.

Anahtar Kelimeler: Hidrojel, vajinal ilaç sistemleri, nanokompozit, kontollü ilaç sistemleri, metformin.

ACKNOWLEDGEMENTS

This thesis research was conducted during the COVID-19 pandemic and took a long time due to both the experimental nature of the research and the challenging conditions of the pandemic. I would like to thank everyone who provided me with support during this period. First of all, I would like to express my deep appreciation to my supervisor, Assoc. Prof. Dr. İsrafil Küçük, for his advice, academic counsel, and support. I would also like to thank the research assistants of Gebze Technical University Institute of Nanotechnology, Ahmet Musap Mert (M.Eng.), Hasan Topaçlı (M.Eng.), Mehmet Emre Aköz (MSc), and Vala Can Aşkan (M.Eng.) for their help in Nano-delight Research Group Laboratory studies. I thank research assistant İpek Ömeroğlu, PhD, for assistance with the Fourier transform infrared spectroscopy experiments; Ahmet Nazım for recording the scanning electron microscopy images; research assistant Ahmet Şenocak, PhD, for performing the differential scanning calorimetry analysis; and Ünal Şen, M.Eng., for overseeing the freeze-drying process. I would also like to thank Burak Erayhan for his help and generous support as a colleague in the laboratory. I would like to thank my co-supervisor, Assistant Professor Dr. Gülengül Duman (Yeditepe University), for her guidance and help. The drug study experiments were conducted with her laboratory team, including her research assistant, Meltem Macit, PhD, who assisted in the pharmaceutical technology laboratory and drug dissolution tests, and technical experts Bilal Şenkal and Mehmet Ali Şenkal, who helped with the freeze-drying and sonication processes (Yeditepe University). I am deeply indebted to Akif Erdoğan for conducting the drug release experiments in the pharmaceutical facility of the R&D department of Sanovel İlaç Sanayi ve Ticaret Anonim Şirketi. Last but not least, I would like to extend my gratitude to my beloved family members, who have always supported and encouraged me throughout my life and in particular while I was performing this M.Eng. research work.

TABLE OF CONTENTS

LIST of ABBREVIATIONS and ACRONYMS

Abbreviations and Acronyms		Explanations
C_0	:	Initial amount of drug in the solution
V_D	:	Dissolution bath volume
(w/v)	:	Weight per volume
A	:	Absorbance
AE-PCOS	:	Androgen Excess and Polycystic Ovary Syndrome Society
C	:	Concentration
C_s	:	Drug solubility
CS 1	:	1% ionically crosslinked chitosan hydrogel prepared manually
CS 2	:	1% ionically crosslinked chitosan hydrogel prepared manually and incorporated with lyophilized egg yolk lecithin
CS 3	:	1% ionically crosslinked chitosan hydrogel prepared manually and incorporated with pure metformin
CS 4	:	1% ionically crosslinked chitosan hydrogel prepared manually and incorporated with lyophilized liposomal metformin
CS/β-GP	:	1% chitosan hydrogel ionically crosslinked with β-glycerophosphate disodium salt
CS	:	Pure chitosan powder
C_t	:	Amount of drug dissolved in a given period of time
D	:	Dilution factor
d	:	Diffusivity of the drug molecules in the substance
DDS	:	Drug delivery system
DLS		Dynamic light scattering
DSC	:	Differential scanning calorimetry
ε	:	Molar extinction coefficient
FSH	:	Follicle-stimulating hormone
FTIR	:	Fourier transform infrared spectroscopy

K_0	:	Zero-order release constant
K_1	:	First-order rate constant
l	:	Path length
LH	:	Luteinizing hormone
M-CS 1	:	1% ionically crosslinked chitosan hydrogel prepared by microfluidics
M-CS 2	:	1% ionically crosslinked chitosan hydrogel prepared by microfluidics, incorporated with lyophilized liposomal nanoparticles
M-CS 3	:	1% ionically crosslinked chitosan hydrogel prepared by microfluidics, incorporated with pure metformin HCl
M-CS4	:	1% ionically crosslinked chitosan hydrogel prepared by microfluidics, incorporated with lyophilized metformin encapsulated liposomal nanoparticles HCl
met: lec	:	Lyophilized metformin encapsulated liposomal nanoparticles
met	:	Pure metformin
MetforminHCl	:	Metformin hydrochloride
Mv	:	Millivolts
NIH	:	National Institutes of Health
nm	:	Nanometre
PBS	:	Phosphate-buffered saline
PCOS	:	Polycystic ovarian syndrome
PDI	:	Polydispersity index
PEG	:	Polyethylene glycol
PVA	:	Polyvinyl alcohol
SD	:	Standard deviation
SEM	:	Scanning electron microscopy
UV-Vis	:	Ultraviolet-visible
v/v	:	Volume per volume
w/w	:	Weight per weight
β-GP	:	β-Glycerophosphate disodium salt
ζ	:	Zeta potential

LIST of FIGURES

LIST of TABLES

1. INTRODUCTION

1.1. Motivation

Polycystic ovarian syndrome (PCOS), which is a syndrome triggered by insufficient follicle-stimulating hormone (FSH) levels during the ovulation period, has attracted great interest as it widely affects many women of reproductive age, approximately between the ages of 14 and 49 [1–3]. In treating PCOS, it is not only important to make lifestyle changes, which include balanced eating and regular exercise; it is also often necessary to use insulin-sensitizing agents such as metformin or pioglitazone to control insulin levels, which influence the levels of luteinizing hormone (LH), androgen, and FSH.

Among these insulin-sensitizing agents, it has been stated in the literature that metformin is the most successful drug in terms of insulin optimization in the treatment of PCOS [2, 3]. However, it has also been noted that there are several side effects as a result of the oral administration of metformin, such as gastric reflux, lactic acidosis, dyspepsia, diarrhoea, nausea, flatulence, and a metallic aftertaste in the mouth [4, 5]. Taking regular high doses of this drug will lead to toxicity. Therefore, the demand for the development of new drug delivery strategies, such as adjusting the dose of the active ingredient needed for treatment or utilizing controlled drug delivery systems (DDSs), has become a significant and frequent topic of research in recent years.

Controlled-release DDSs enable the release of a drug in a controlled manner for an extended period without losing its therapeutic effects. Controlled release entails manipulating the release of the drug, and so the drug may be released in a specified part of the body. Controlled-release DDSs use several mechanisms including diffusion, chemical reactions, solvent activation, and transport. In the case of diffusion, polymeric matrices are usually used as reservoirs for a selected drug or a particular material may be used to distribute the drug homogeneously. In the presence of chemical reactions during drug delivery, biomaterials cause degradation of the delivery vehicle while interacting with water or other agents. In the solvent delivery mechanism, materials that swell in the presence of water are used to release

the drug, which is preserved in the vesicle capsule or with the presence of an osmotic effect [6].

Nanoparticles, hydrogels, microgels, and micelles have been used for encapsulating drugs for slow release in the targeted area. To enhance the controlled release of a drug, several parameters are crucial, including the location of administration, the drug itself, the dosage of the drug, and the polymer choice, and these variables must be considered carefully [7]. Due to their enhanced characteristics, composite nanostructures that aim to control the release of drugs are successful candidates for eliminating the potential side effects of the active ingredient, avoiding overdosages, and lessening the frequency of drug administration [4],[5]. Stimuli-responsive 'smart' hydrogel systems are chosen for biomedical applications due to their high biocompatibility and low cytotoxicity. Both natural and synthetic polymers have been used to fabricate responsive hydrogel systems for biomedical purposes. Natural polymers, or biopolymers, which include those that are polysaccharide-based, such as chitosan, alginate, and their composite derivatives, are commonly used for biomedical applications. These polymers are highly biocompatible and broadly used in DDSs and implant applications. Synthetic polymers, such as polyethylene glycol (PEG), polyvinyl alcohol (PVA), peptides, poloxamers, and other synthetically derived polymers, have also been used for biomedical applications [8]. Crocini et al. fabricated PEG hydrogel scaffolds with adjustable stiffness and successfully mimicked physiological microenvironments for tissue engineering applications [9].As composite derivatives, the PVA-alginate hydrogel systems designed by Golafshan et al. were used for wound healing, and the results showed that acceleration of the healing process was achieved [10]. Hydrogel forms of these polymers have also been used for controlled DDSs [11].

It is vital to consider fabrication methods in the production of the highly biocompatible, viscous, and biodegradable hydrogels (e.g., chitosan) used in controlled DDSs because they directly affect drug release performance [12]. Therefore, the choice of production methods with which the structural properties of hydrogels can be easily manipulated is important in the design process of controlled DDSs [10]. Various production methods including batch emulsion, lithography, microfluidics, and mechanical fragmentation are used for hydrogels [13]. Although these conventional production methods enable the production of micro- and nanomaterials, such as liposomes [14] and hydrogel nanocomposites [15], which have been used for

biomedical applications as a result of their varied geometrical shapes including films, particles, and three-dimensional shapes, there have also been problems in the production of their controllable features, such as problems with the precise control of their sizes, shapes, monodispersity, and mechanical stability [16]. Microfluidic systems are innovative systems that are preferred for their advantageous production features, which enable their parameters, such as flow rate or viscosity, to be altered for ease of production [16]. Several types of microchannel design junctions are available for microfluidic devices, such as Y-junction and T-junction designs, which are named according to their merging geometry [17]. As a result of focusing the flow, V-shaped and T-shaped microfluidic systems are suitable for the production of drug-loaded hydrogels, with their simple designs allowing for the creation of highly monodispersed microbubbles together with the joining of micron-sized channels that carry different fluids through them [18, 19]. High monodispersity and diameter size are vital parameters for DDSs, depending on the fluid's viscosity and relative velocity [15, 17, 20].

In terms of controlled DDSs, hydrogel platforms for therapeutic applications, which include metal nanoparticles, clays, carbon-based materials, metal oxides, and polymeric nanoparticles such as niosomes and liposomes, are used as micro/nano hydrogel systems [14, 15]. High stability, high biocompability, and low toxicity are desired in DDSs. Therefore, liposomes are the vesicles chosen for controlled drug delivery applications. These vesicles have one or more phospholipid bilayers. Thus, hydrophilic and hydrophobic drug loading can be performed using liposomes, since they have a hydrophilic core and hydrophobic bilayer [15, 21]. As mentioned previously, injectable stimuli-responsive hydrogel platforms have also been used for DDSs. According to the drug administration route, the choice of polymer may vary depending on various parameters, such as the physiological conditions of the targeted area (pH or temperature stimuli-responsive), and the gelling mechanism must also be taken into account [22]. For vaginal drug administration, viscous polymers are used due to the fact that they possess retention in vaginal mucus, because the vaginal environment tends to clear itself via vaginal secretions. Moreover, leakage of the administered drug can be avoided [23]. Vaginal drug administration is preferred because of its localized effects and elimination of the first-pass effect and other side effects that are caused by the gastrointestinal system [23, 24].

1.2. Objective of the thesis

The research presented here was undertaken with the aim of generating drug-loaded liposomes incorporated into thermo-sensitive composite chitosan hydrogel platforms produced via microfluidics for topical applications. These composite hydrogel systems are intended for use in topical applications for the treatment of specific disorders such as PCOS. The hydrogel platforms produced by means of microfluidics are designed to have monodisperse microbubbles with homogeneous porous structures so as to achieve controlled drug release. As a drug delivery study, in vitro drug dissolution testing results and loading efficiency are also evaluated.

1.3. Scope of the thesis

This thesis was planned with the aim of producing thermo-sensitive hybrid hydrogel platforms for topical applications of vaginal drug administration to treat PCOS and other hormonal diseases without any side effects. A T-shaped microfluidic system was chosen for the production of the thermo-sensitive hydrogel composite delivery system (chitosan and β-glycerophosphate incorporated with metformin-loaded liposomes) with a high rate of uniform pore size and size distribution displaying a low polydispersity ratio (PDI). It was aimed to observe the controlled drug release of the drug alone and while using drug-loaded liposomes of the desired morphology and size. Characterization techniques were applied to the produced hydrogels. The dynamic light scattering (DLS) technique was used to obtain data about the zeta potentials and diameters of the produced nanoparticles (drug-loaded and unloaded liposomes), while scanning electron microscopy (SEM) was used to determine the morphology of the produced bare or drug-loaded liposomes and hydrogels. Differential scanning calorimetry (DSC) was used to collect data about how the physical properties of the produced hydrogels change over time. Fourier transform infrared spectroscopy (FTIR) was used to determine whether any chemical deformation or contamination took place. SEM was also used to observe drug entrapment and the diameters of the hydrogels and liposomes. Statistical analysis was also performed (one-way analysis of variance). Hence, an in vitro drug release study is presented here. In the future, in vivo studies for PCOS treatment applications can

be performed with the proposed composite hydrogel structures, and this research can also be used as a model for further preliminary studies in this field. Additionally, the V-shaped microfluidic method can be applied to incorporate drug-loaded liposomes into hydrogel composites to be utilized for the treatment of PCOS. Such an approach has not been developed yet, signifying the novelty of this thesis.

2. LITERATURE REVIEW

2.1. Polycystic ovarian syndrome and its treatment strategies

The prevalence of PCOS, which is an endocrine disorder, has been reported to range between 8% and 13%. It is seen in women of reproductive age, roughly between 14 and 44 years of age [25, 26]. Several studies have been conducted to confirm the prevalence of PCOS based on the criteria of three main institutions, namely the National Institutes of Health (NIH), the Rotterdam ESHRE/ASRM Sponsored PCOS Consensus Workshop (Rotterdam Criteria), and the Androgen Excess and Polycystic Ovary Syndrome Society (AE-PCOS) [25, 27]. This hormonal disorder can be explained sequentially, whereby with the secretion of increased LH from the hypothalamus, the serum testosterone level also increases. This secreted hormone, or androgen, is subsequently converted into oestrogen. Thus, these increases in hormone levels lead to the production of increased LH and the continued looping of this mechanism is inevitable [28, 29].

The most commonly reported PCOS symptoms are irregularities in the menstrual cycle, hyperandrogenism, and insulin resistance, which causes hormonal disorders that lead to diabetes. Women who are diagnosed with PCOS are negatively affected by these symptoms, which damage their quality of life [30, 31]. It has been observed that LH is secreted by the hypothalamus at an above-average rate in patients with PCOS. This increase in the LH level leads to an increase in the LH/FSH ratio, causing the FSH level to be insufficient for the growth of the follicles that are necessary to initiate the menstrual cycle [28]. Thus, follicle growth is inhibited, causing the roots of the underdeveloped follicles to accumulate in the ovaries, which results in a further deficiency in FSH, which is vital for sustaining the natural growth of the follicles (Figure 2.1), [29, 32].

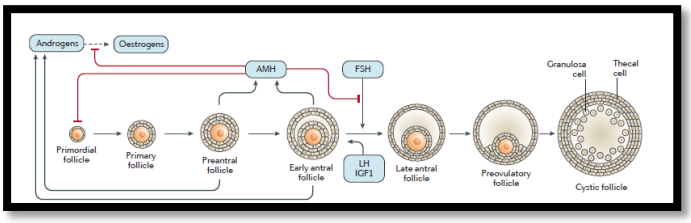

Figure 2.1: Ovarian follicular behaviour in PCOS [33].

In the literature, several treatment strategies have been applied to control and balance the insulin level of patients with PCOS [34]. Physicians have proposed lifestyle modifications, such as diet and exercise programs, and if that is not sufficient, medication is also suggested [26, 35, 36]. Moreover, combinations of both lifestyle modifications and drug treatment are often used in the treatment of PCOS. The combination of treatments will differ from patient to patient, as patients with PCOS must first prevent weight gain, and then a diet and exercise program with an insulin-sensitizing drug may be suggested. If the patient has both PCOS and infertility issues, drug combinations for anovulation will be recommend [27, 29, 37]. Treatment varies based on the patient's age, ethnicity, genetics, and other factors [27].

Insulin is a crucial parameter because it causes a hormonal imbalance when increased levels are present in the blood serum. Therefore, for the treatment of type II diabetes, insulin balancers and controllers are used, including medications such as metformin, rosiglitazone, pioglitazone, and D-chiro-inositol [38]. Metformin is the most commonly preferred insulin-sensitizing drug for type II diabetes and studies have shown that it also helps with ovarian oestrogen secretion, reducing the androgen levels. Thus, metformin decreases the level of insulin, which negatively impacts the testosterone levels of PCOS patients [5, 39].

2.2. Controlled drug delivery and strategies for PCOS

Controlled DDSs were introduced for the sustained release of oral and transdermal therapies in the early 1950s, and then new drug release strategies such as zero-order release systems, DDSs based on microtechnology, and nanotechnology applications were subsequently developed. With time, new controlled DDSs and various other novel systems including micro reservoir implants, transdermal patches, nanoparticles, antibodies, and microneedles were developed [40]. Controlled drug systems are more highly preferred than conventional DDSs. The reason for this preference is in conventional DDSs burst release of the drugs takes place that has not an ability to control release of drugs, however; control drug delivery systems like nano vehicles may allow control release of administrated drugs that provides desired an efficacy of drugs. In addition, drugs at higher concentrations are generally preferred for quick treatment responses, leading to increases in cytotoxicity and side effects [40]. Controlled-release DDSs are convenient systems that improve the bioavailability of drugs by hindering premature degradation. This helps to sustain drug concentrations in the therapeutic ranges without any possible adverse effects [41]. This technology also enables different drug administration routes. For the treatment of PCOS, conventional oral pills have traditionally been used, as described in Chapter 1.1. However, alternatives to oral drug administration, such as vaginal drug administration, are also available for PCOS treatment [42].

For vaginal drug delivery, mucoadhesion is a critical feature in efforts to achieve efficient treatment. Mucoadhesion is described as the state in which two materials bind for a prolonged period of time with force, or interfacial binding. If one of these two materials has an appropriate physiological nature (mucosal or epithelial), then this phenomenon is called bioadhesion [43]. Smart biomaterials, such as stimuli-induced hydrogels, liposomal patches, and polymeric micelles, are chosen for mucoadhesion to deliver drugs with carrier platforms like hydrogels due to their excellent carrier capacity and retention time at the targeted site [44]. Thus, the mucosal environment provides drug administration routes with in situ mucoadhesive gelling DDSs. In situ gelling polymers are accordingly used for this type of drug delivery. For example, chitosan polymers are used for oral, ocular, buccal, and intravaginal drug delivery due to their mucoadhesive properties [23]. In the literature, chitosan has been studied for in situ hydrogel DDSs. The addition of gelling agents

makes chitosan stimuli-responsive due to crosslinking. For instance, using a β-glycerophosphate crosslinker makes chitosan a thermally responsive hydrogel system with electrostatic crosslinking [45]. Chitosan furthermore has hydrochloride and amino radical groups, which give rise to the form of hydrogen and covalent bonding. Scientists have found that in environments with low pH, amino groups undergo protonation, which causes them to have a positive charge when interactions occur with the negatively charged elements (sialic acid due to the presence of carboxylate group) of mucins, which comprise epithelial cells of the mucosal tissue. This affects the solubility of chitosan. In particular, hydrogen bonding plays a critical role in the mucoadhesion of chitosan [46].

Hydrogels and nanoparticle incorporations have been used to maintain the bioavailability of drugs. Although nanotherapeutics are successful candidates for targeted DDSs with proper modifications, only a small percentage of nanotherapeutics can accumulate in targeted areas due to hepatic clearance. Therefore, to improve the retention times of drugs, carriers like hydrogel platforms are chosen to enhance drug bioavailability as a result of their stimuli-responsive nature and their biocompatibility for controlled DDSs targeting specific areas [42, 43].

Metformin hydrochloride is an important drug in the treatment of PCOS. To improve the oral bioavailability of metformin hydrochloride, Manconi et al. studied a hybrid chitosan-based thermo-sensitive hydrogel, which was incorporated with drug liposomes [47]. Moreover, Saini et al. studied the intravaginal drug administration of metformin-loaded niosomes, which were merged with thermo-sensitive chitosan hydrogel platforms and used successfully for the treatment of PCOS [42].

2.3. Composite hydrogels in controlled drug delivery

Over the years, with the developments in nanotechnology and biotechnology, composite nanomaterials have been studied and designed for controlled and targeted drug delivery. Hybrid nanocomposite materials are composed of both organic and inorganic components with sizes that range from a few angstroms to tens of nanometres. Hybrid nanomaterials are preferred for advanced biomaterial applications due to their highly improved features, and particularly their mechanical and thermal stability. Porosity, for example, is an important variable in drug delivery,

cell therapy, and tissue regeneration because it allows materials to act as scaffolds. Numerous organic and inorganic hybrid hydrogels are used as functional materials for drug delivery and tissue engineering [48]. Hydrogel nanocomposites are smart materials with improved features, and due to their stimuli-responsive behaviours, they are good candidates for drug delivery applications [49, 50]. In terms of stimuli-responsiveness, both internal and external parameters (e.g., pH, temperature) trigger drug release [49]. Studies have shown that the aim of using composite hydrogels in DDSs is generally the controlled release of a drug and, hence, the bioavailability of that drug. They can be incorporated using different types of nanoparticles, such as nanofibers, nanometals, nano-biomaterials, and liposomes [49, 50]. Additionally, drugs could be loaded into nanoparticles in the hydrogel scaffold or directly into the scaffolding medium [51].

Among liposome particle-based hydrogels, hybrid hydrogels known as lipogels are used for DDSs [52]. Liposomes are vesicles that are predominantly used for pharmaceutical and cosmetic applications (Figure 2.2). These vesicles are composed of natural non-toxic phospholipids and cholesterol [53, 54]. The carriers are particularly valuable in terms of the biocompatibility of controlled DDSs. Both hydrophilic and hydrophobic drug loadings have been studied [31, 32].

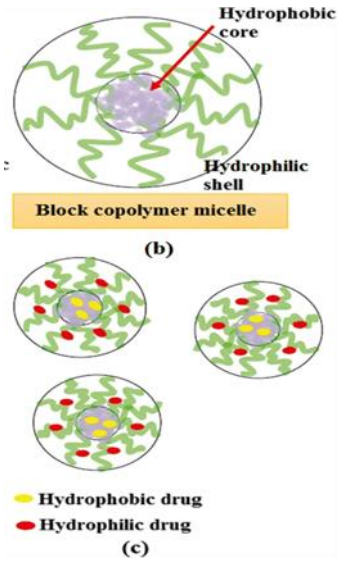

Figure 2.2: Structure of a nanoliposome loaded with both lipophilic and hydrophilic drugs [54] .

Liposomes can easily be absorbed from cell membranes due to their structures being similar to those of the cells. Since cellular uptake will be accelerated, the

targeted drug delivery can be accomplished [55]. Liposomes, therefore, are valuable for controlled DDSs [56]. Merging these drug-loaded micelle structures with hydrogels provides the desired dose manipulation along with the controlled release of the drug.

2.4. Microfluidic Systems

Microfluidics constitute an ideal system for ensuring the conditions of precision fluid control and the fast fabrication of structures with diameters on the micron and sub-micron scales [57]. Microfluidic systems are used for the generation of drug-loaded hydrogel systems because they are more effective compared to traditional fabrication methods, which include sonication processes, crosslinking, batch emulsion, lithography, electrohydrodynamic spraying, and mechanical fragmentation [13, 14].

The above-mentioned methods are known as conventional methods, which have limitations in terms of facilitating research for practical applications. Although these fabrication methods yield nano-sized particles in various size ranges, high PDI values may also be indispensable [58]. In terms of controlled DDSs, the monodispersity of particles must be considered in light of drug dosage levels [42].

Microfluidic systems are promising systems that are both one-step and economical, and they provide the possibility of continuous production with minimized amounts of material [59]. In the literature, some studies have concentrated on hydrogel drug transportation systems in which particles have high monodispersity and homogeneity [43, 44]. As noted above, different types of junctions have been used before in microchannel microfluidic devices, such as Y-junctions and T-junctions, based on merging geometry (Figure 2.3) [16, 60].

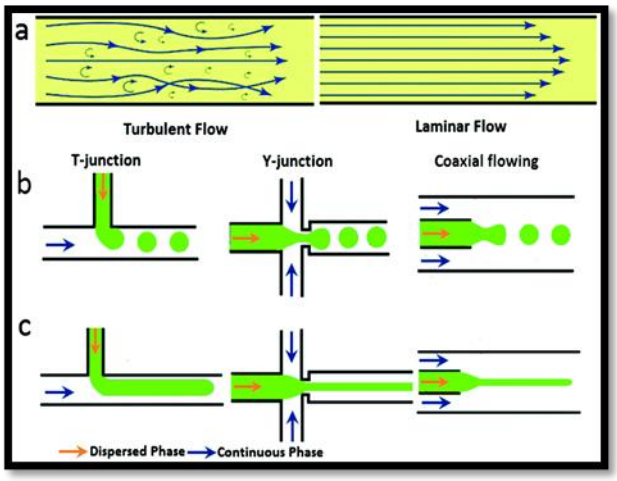

Figure 2.3: Schematic representation of the three main types of junctions of microfluidic systems (b) and (c) with two basic fluid dynamic behaviour channels (a) [60].

Flow-focusing approaches, particularly within V-shaped and T-shaped microfluidic systems, can be used for the production of drug-loaded hydrogel platforms with high monodispersity using fluid mechanics with micron-sized channels [13, 16, 17].

Regarding microfluidics, highly monodispersed carrier platforms have been fabricated to offer precise control in terms of flow rate and velocity of the fluids. For instance, nano-sized hydrogel platforms have been used to produce micro- and nanocarriers. Their stimuli-induced natures allow them to be used for various biomedical applications (e.g., drug delivery, cell encapsulation, and biosensors) [48, 61]. Moreover, the microfluidic fabrication technique has been studied for use with liposome vesicles for drug delivery applications. It is known that biopharmaceuticals have limited storage lives. Thus, liposomes are used to prolong the half-life of the drugs. Microfluidically fabricated drug-loaded liposomes have shown higher drug encapsulation efficiency when compared to conventional ones [21, 62, 63].

This thesis presents the microfluidic production of liposomal nanoparticles incorporated with injectable thermo-sensitive chitosan-based hydrogel carriers. The thesis comprises three major sections. The first section reviews the production of drug-loaded nanoparticles, utilizing probe sonication and freeze-drying. This leads to a reduction in the sizes of the drug particles. Decreasing the size of the nanoparticles helps to avoid potential side effects of metformin as well as reducing the dose

frequency of the drug. The second section of the thesis focuses on the generation of electrostatically crosslinked thermo-sensitive chitosan-based hydrogels via conventional and microfluidic methods, with characterization of the raw materials used and the resultant samples. The third section presents the drug dissolution study and investigates drug dissolution behaviour in an artificially formed vaginal solution environment. In vitro studies as well as in vivo studies are crucial in terms of providing novel approaches for controlled drug delivery by tuning the process parameters for further developments.

3. MATERIALS & METHODS

This chapter presents the materials and devices that were used in this thesis research and the experimental procedures that were conducted. The production methodology of both liposomal nanoparticles and nanocomposite hydrogel platforms via conventional and microfluidic synthesis and the analytical work are described in detail. Experimental procedures, preparation, and characterization methods for liposomal nanoparticles, chitosan polymeric solution, and chitosan-based thermo-sensitive nanocomposite hydrogel platforms are described. The statistical analysis of the experiment is also described.

3.1. Materials

The precursor materials used in the experimental works are shown in Table 3.1. Chitosan polymer was used for thermo-sensitive hydrogel production. Acetic acid was also used for better dissolution of chitosan because chitosan, having a degree of deacylation of 75%, is not water-soluble; therefore, acetic acid (glacial) was added to the chitosan polymer solution as described in Chapter 3.2.2. In order to produce liposomal nanoparticles, L-α-lysophosphatidylcholine (egg yolk lecithin, ≈60% (TLC)) and metformin HCl were used. Metformin HCl was the drug to be encapsulated and egg yolk lecithin was the lipid for nanoliposomal vehicle preparation. By prone sonication, metformin encapsulated liposomal nanoparticles particles were achieved. β-Glycerophosphate disodium salt powder was used as a gelling agent. The salt solution was added to the chitosan polymer solution to generate thermo-sensitive hydrogel platforms as described in Chapter 3.2.2.

Table 3.1: Materials used in all experimental works of this research.

Material	Brand	City/Country
Chitosan from shrimp shells, ≥75% (deacetylated)	Sigma-Aldrich	Schnelldorf/Germany
L-α-Lysophosphatidylcholine (egg yolk lecithin, ≈60% (TLC))	Sigma-Aldrich	Schnelldorf/Germany
Metformin hydrochloride (metformin)	Merck	Darmstadt/Germany
Acetic acid (glacial)	TEKKİM	Bursa/Turkey
β-Glycerophosphate disodium salt	Biosynth Carbosynth	Compton/UK

3.2. Methods

3.2.1. Preparation of liposomal nanoparticles with/without metformin

Metformin HCl (2.5 mg) and egg lecithin (2.5 mg) were weighed separately and then dissolved in 5 mL of pure water together. The prepared solution was then placed in an ice bath. The ice bath was placed onto a lifting platform to prevent the degradation of the liposomes and metformin during the probe sonication process (BANDELIN SONOPULS HD 2070, Germany) (Figure 3.1). Sonication time was kept at 15 min with 5 cycles and 72% power was applied. Liposomal nanoparticles without metformin were similarly prepared. Subsequently, samples were kept in a

freezer (Ultra-Low Temperature Freezer U570 Premium, Germany) at -80 ℃ for 1 day to preserve their stability (Figure 3.1). Lastly, the samples underwent a freeze-drying process (CHRIST ALPHA 1-4 LD, Germany) for both characterization and dissolution of the drug (Figure 3.1). The lyophilization process was performed to prevent oxidative degradation and sustain the chemical stability of the liposomal nanoparticles.

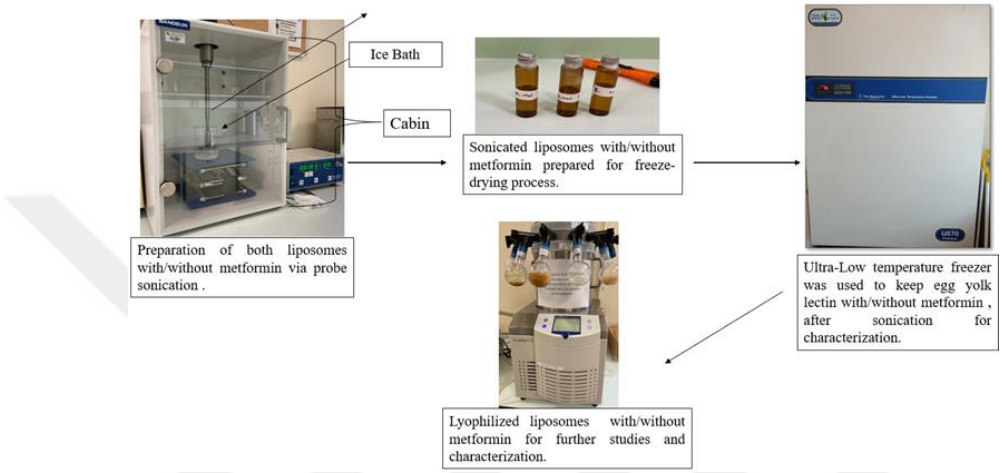

Figure 3.1: a) Sonication device used to sonicate drug and liposomal nanoparticles, b) samples for freeze-drying process after sonication, c) -80 ℃ freeze-dryer for keeping the samples for further studies, and d) lyophilized samples used.

3.2.2. Manual preparation of thermo-sensitive chitosan-based hydrogels incorporated with metformin-encapsulated liposomal nanoparticles

A chitosan solution (1% (w/v)) was prepared by dissolving chitosan powder in distilled water for 15 min with moderate stirring (1000-1550 rpm) at 37 ℃ (Figure 3.2). For complete dissolution of the chitosan powder, 1% acetic acid was added with a 2.50 micropipette drop by drop at 1500 rpm and 37 ℃ with the solution on a magnetic stirrer for 1 h. The pH of the chitosan solution was kept at 3.5-4 ℃. Before achieving a transparent chitosan solution with the desired pH, pre-formulations were conducted.

Meanwhile, an 80% (v/v) β-glycerophosphate disodium salt solution was prepared with distilled water as a crosslinker solution. This β-glycerophosphate solution was kept in a refrigerator for gelation. After 1 h of stirring, the chitosan solution was also placed in the refrigerator. For ionic gelation, cold glycerophosphate solution was added to the chitosan solution with a volume ratio of 1:1 (v/v) drop by drop in an ice bath (Figure 3.2).

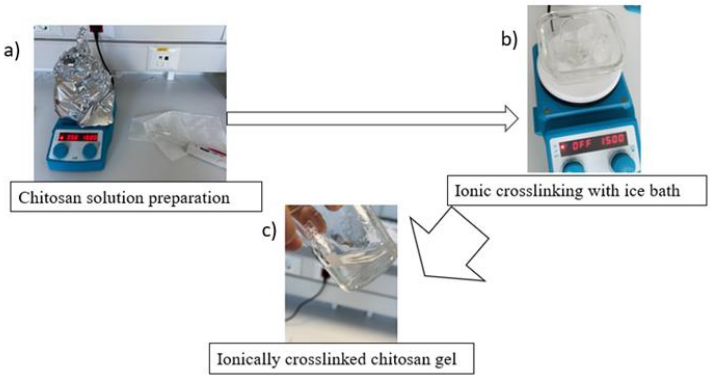

Figure 3.2: a) Dissolving chitosan powders in pure water/acetic acid solvent for preparation of the chitosan solution, b) addition of the gelling agent salt solution into the chitosan solution for ionic crosslinking, c) ionically crosslinked chitosan gel obtained via conventional method.

Ionic interactions occurred between the positively charged chitosan solution and negatively charged groups of the β-glycerophosphate solution. After gelation, hydrogels were placed in a vacuum oven for 1 h at 30 ℃ under pressure of 70 mPa (model CLRC-17, CLS Scientific, Turkey). From the vacuum oven, they were moved to a refrigerator at 4 ℃ to await characterization and drug release studies. After this stage, lyophilized egg lecithin particles, which were sonicated with metformin at 1:1 (w/w), were incorporated with hydrogels. Finally, the incorporated hydrogels were stored for drug release studies and lyophilized for characterization.

3.2.2.1. Characterization of the polymer solution

The chitosan polymer solution was optimized with different strategies. Different concentrations of chitosan solution and crosslinker solutions were prepared while the

acid concentration was kept at 1% (v/v). The characterization of the pH of the gel solution was measured before and after the addition of the crosslinker. The appearances of the chitosan solution and the gel solution (chitosan β-glycerophosphate) before the gelling agent were also noted. The desired appearances and pH values of the polymer were evaluated in an experimental study. Viscosity, density, and surface tension of the chitosan polymer solution were measured, as well. This experimental study was not focused on the optimization of the microbubble size of the chitosan polymer solution. Therefore, a single formula and single temperature were selected while investigating the drug encapsulation efficiency of the metformin encapsulated liposomal nanoparticles incorporated with hydrogel platforms.

The viscosity of the polymer solution was measured at 23 ℃with the tuning fork method by immersing the plates in the device in a 50-mL dispersion cuvette (model SV-10, Vibro Viscometer, A&D, Japan) at least three times. Before the measurements, 40 mL of 1% chitosan solution was prepared for precise measurement. Thereafter, the chitosan polymer solution (1% (w/v)) was poured into the dispersion cuvette (Figure 3.3). The viscosity of the solution was determined according to temperature values and all data were recorded.

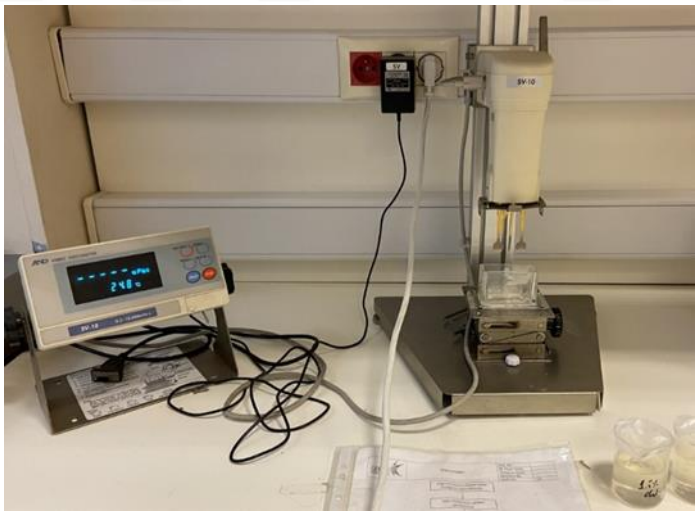

Figure 3.3: Experimental viscometer set-up for measuring polymer viscosity.

The density of the chitosan polymer solution (25 mL, 1% (w/v)) was evaluated with a pycnometer (Pycnometer Density Bottle Meter, ISOLAB, Germany). The empty weight of the pycnometer was noted as 29.925 g and then 25 mL of the 1% chitosan

solution was poured; 55.147 g was obtained as the total weight of the pycnometer a and the solution (Figure 3.4). The difference reveals the weight of the polymer and Eq. 3.1 was used to calculate the density of the polymer solution:

$$d = \frac{m}{V} \tag{3.1}$$

Here, d is density (g/cm^3), m is the mass of the sample (g), and v is volume (cm^3). Using Eq. 3.1, we can evaluate the density of the 1% chitosan polymer solution as shown in Eq. 3.2:

$$D = \frac{m}{V} = \frac{(55.147 - 29.925)g}{25\ mL = 25cm^3} = 1.008\frac{g}{cm^3} \tag{3.2}$$

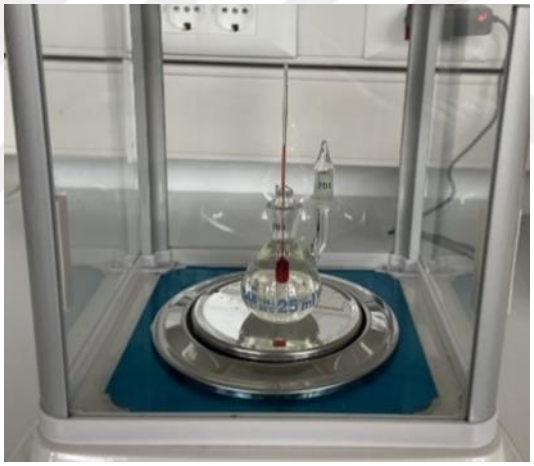

Figure 3.4: Density measurement of chitosan polymer solution by pycnometer.

The surface tension of the 1% (w/v) chitosan polymer solution was measured with a contact angle device (Theta Contact Angle Meter, Attension, Biolin Scientific, Sweden) with measurement sensitivity of ± 0.1 mN/m. The needle of the device was used to evaluate the surface tension of the solution. As the drop falling from the tip of the needle broke, a cross-sectional area was generated and the surface tension was evaluated by calculating the gap at the break.

3.2.3. Microfluidic preparation of thermo-sensitive chitosan-based hydrogel incorporated with metformin-encapsulated liposomal nanoparticle

The chitosan (1% (w/v)) and β-glycerophosphate crosslinker solutions were prepared as described in Chapter 3.2.2. After the preparation of the chitosan solution, the solution was filtered with a 0.45-µm syringe filter (Cellulose Acetate Syringe, GVS Filter Technology, UK) to eliminate the undissolved particles and thus prevent clogging while feeding the polymer solution into the microchannel. The polymer solution was added with a 10-mL BD plastic syringe (Becton Dickinson, USA) together with digitally piston-controlled pumps (IPS-14-RS, Inovenso, USA). A T-shaped microfluidic junction was used (Figure 3.5).

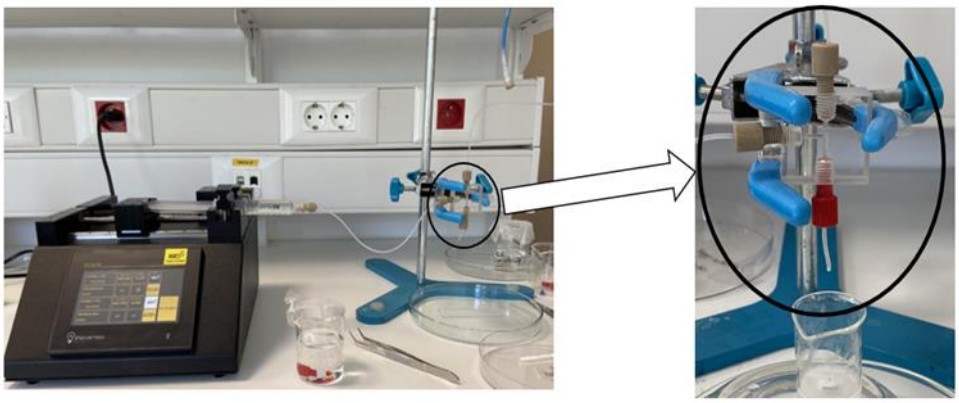

Figure 3.5: Microfluidic experimental set-up.

In this microfluidic system, two immiscible phases were used to achieve microbubbles formed through the junction section of the microchannels. The chitosan solution was applied as the continuous phase, while the dispersed phase was gas flow (nitrogen gas). The liquid flow rate was kept at 200-220 µL/min under the flow of pure gas and the pressure applied during bubble generation was 10-15 bar at 25 ℃ ambient temperature. The system was allowed to form uniform continuous bubbles. Due to the gravitational force, the microbubbles create a weight drop then collected in a beaker. The volumetric ratio of polymer solution to crosslinker solution was kept at 1:1 (v/v) for ideal gelation (Figure 3.6). After the generation of microbubbles, the

crosslinker solution was added to the collected bubbles drop by drop in an ice bath. Once gelation was achieved, hydrogels were placed in a vacuum oven for 1 h at 30 ℃ under pressure of 70 mPa (CLRC-17, CLS Scientific, Turkey).

Under vacuum, the air inside the hydrogels was removed and the hydrogels were kept in a refrigerator at 4 ℃ to await characterization and drug release studies. In the final step, the incorporation of lyophilized drug-loaded liposomes was achieved with the same procedure described in Chapter 3.2.2).

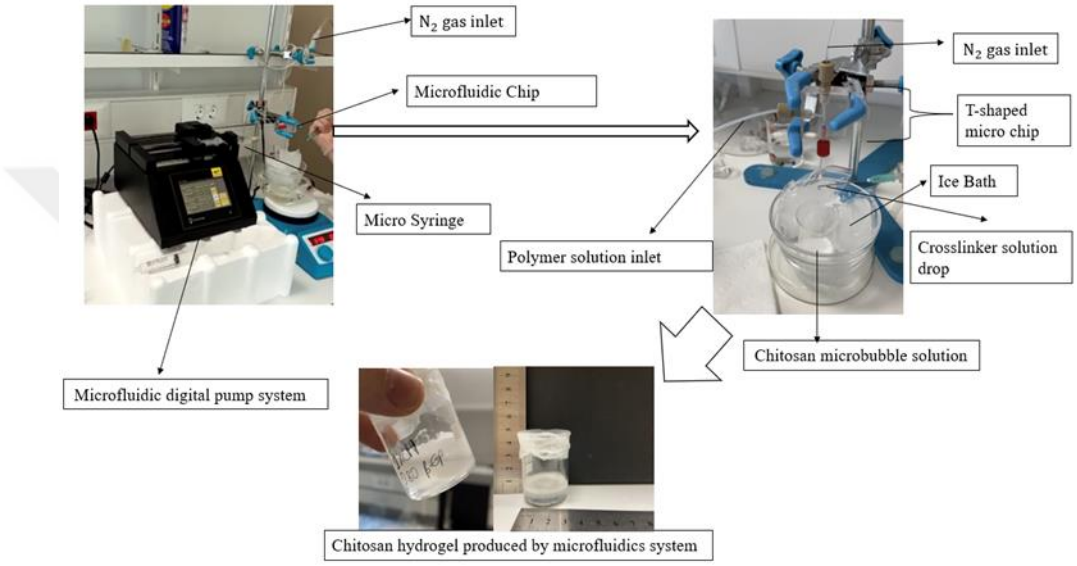

Figure 3.6: Preparation of ionically crosslinked chitosan hydrogel with microfluidic system.

3.2.4. Microbubble characterization of microfluidically produced chitosan hydrogel

The morphology of the microbubbles produced by the T-junction microfluidic device was evaluated using an optical microscope (AxioCam MRc 5, Zeiss, Germany) (Figure 3.7). A small amount of freshly generated chitosan microbubbles was collected on glass slides at the outlet channel of the T-junction microfluidic device. The size measurement of bubbles was done just after generating them from the microchannel. For precise evaluation of the images, 5× and 10× objective lenses were used for magnification. Microbubble diameters were determined and the images were recorded.

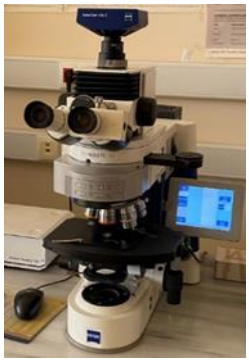

Figure 3.7: Optical microscope used for microbubble characterization.

3.2.5. Kinetics of metformin release

After performing dissolution tests, the collected data were reviewed considering the controlled drug delivery profile. For evaluation, mathematical models of drug kinetics were used (zero-order, first-order, and Higuchi model) and one-way analysis of variance (ANOVA) was applied, followed by Tukey's analysis [64].

3.2.5.1. Evaluation of metformin HCl drug release profile in dissolution medium with mathematical models

Model-dependent methods use different mathematical functions to define the dissolution profile of a drug. Such model-dependent approaches include zero-order, first-order, Hixson-Crowell, Korsmeyer-Peppas, Baker-Lonsdale, Weibull, Hopfenberg, Gompertz, and regression models [65].

3.2.5.2. Zero-order kinetics model

This model is used to express drug dissolution profiles for specified dosage forms that do not have the tendency to break down and show slow-release profiles. The following equation is applied:

$$C_0 - C_t = K_0 t \qquad (3.3)$$

Equation 3.3 can be rearranged to calculate the amount of drug dissolved in a specified period of time, as seen in Equation 3.4:

$$C_t = C_0 + K_0 t \quad (3.4)$$

Here, C_t is the amount of drug dissolved in period of time t, C_0 is the initial amount of drug in the solution, and K_0 is the zero-order release constant (concentration/time) [65].

3.5.2.3. First-order kinetics model

This drug model is used for describing drug dissolution release in pharmaceutical dosage forms such as those containing water-soluble drugs in porous matrices. The first-order kinetics release model is expressed by the following equations:

$$d_C/d_t = -K_1 C \quad (3.5)$$

$$\log C = \log C_0 - K_1 t/2{,}30314 \quad (3.6)$$

Here, C_0 is the initial concentration of the drug, K_1 is the first-order rate constant, and (t^{-1}) is the time [64].

3.5.2.4. Higuchi model

This mathematical model was suggested by Higuchi in 1961 as the first mathematical model describing drug dissolution profiles in matrix systems. This model was derived based on several hypotheses:

- The initial drug concentration in the matrix is much higher than the drug solubility.
- Drug diffusion takes place in only one dimension (edge effect should be avoided).
- Drug particles are much smaller than the thickness of the system.

- The swelling matrix and dissolution are small or negligible.
- Drug diffusivity is constant.
- Perfect sink condition is always attained in the release environment.

Accordingly, this model is given by Eq. 3.7 [65]:

$$f_t = C = A\sqrt{d\,(2C - C)C_s t} \tag{3.7}$$

is the amount of drug released in time t per unit area A, C is the initial drug concentration, C_s is the drug solubility in the matrix medium, and d is the diffusivity of the drug molecules in the substance. The following simplified version of Eq. 3.7 is known as the simplified Higuchi model [65]:

$$f_t = C = K_H \times t^{1/2} \tag{3.8}$$

3.2.6. Statistical analysis

Calculations of mean values and average standard deviations (SDs) were performed using Microsoft Office Excel. The results were expressed as mean ± SD. Data analysis was performed using GraphPad Prism Version 5.04. Statistical analysis of dissolution data was performed by one-way ANOVA followed by Tukey's analysis (n=3), and $p<0.05$ was assumed to be statistically significant [66].

3.2.7. Determination of loading efficiency of metformin

For calculating the percentage of the active substance (metformin) loaded into the liposome vesicles, UV-Vis analysis was conducted based on a literature review [67–69]. Stock solutions of 2.5 mg of metformin in 10 mL of pure water and 5 mg of freeze-dried met: lec (1:1) samples in 10 mL of pure water were prepared. Subsequently, solutions were transferred to two different centrifuge tubes to prepare the sample solutions, and the tubes were filled to 50 mL with pure water. Next, ultracentrifugation was performed for 4 min for each sample to separate vesicles from unentrapped active substance. Absorbance values were evaluated using a quartz cuvette [69] and then loading efficiency was evaluated.

3.2.8. Characterization of liposomal nanoparticle size with dynamic light scattering (DLS)

The mean particle size of the liposomal nanoparticles, zeta potential (ζ), and PDI values were evaluated by dynamic light scattering (DLS; Zetasizer Nano ZSP, Malvern Instruments, UK) with Zetasizer Software Version 7.12. Briefly, small amounts of lyophilized, empty liposomal dispersions and the drug-incorporated version of them were prepared for measurements. In each measurement, slightly turbid suspension was required, and the dispersions to be measured were transferred to disposable folded capillary cells. Cells were placed into the device at a 90° angle (Figure 3.8). The measurements were conducted at room temperature (approximately 25 ℃) in triplicate for accurate data evaluation.

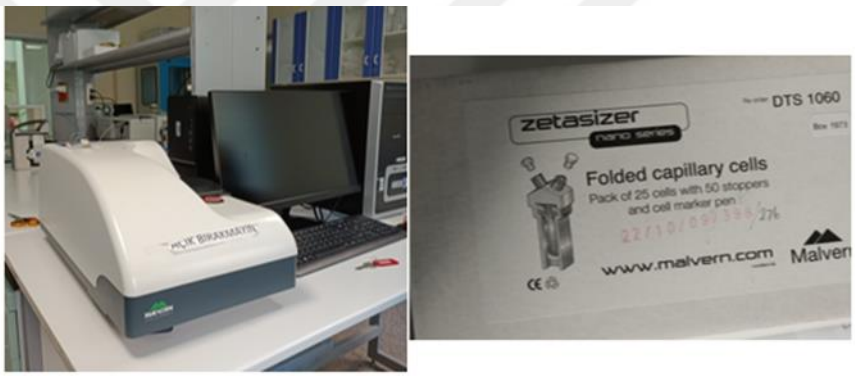

Figure 3.8: Dynamic light scattering device and capillary cells used for DLS.

3.2.9. Chemical analysis of produced liposomal particles and nanocomposite hydrogels with Fourier transform infrared spectroscopy (FTIR)

Lyophilized liposomal nanoparticles with and without the drug, pure chemicals, and hydrogels, which were generated with two different methods and incorporated with nanoparticles, were subjected to FTIR analysis to investigate drug presence and the interactions of the compounds after incorporation of nanoparticles by observing the shifts in wavenumbers. Approximately 3 mg of each sample was placed in the spectroscopy chamber (Spectrum 100, PerkinElmer, USA) and wavenumber measurements were done in the range of 600-4000 cm^{-1}.

3.2.10. Thermal property analysis of produced liposomal nanoparticles and nanocomposite hydrogels with differential scanning calorimetry (DSC)

The thermal properties of the samples were analysed with a differential scanning calorimeter (DSC 404 C Pegasus, Netzsch-Gerätebau GmbH, Germany). The lyophilized liposomal nanoparticles (empty liposomes and liposomes combined with the drug), dust-like pure chemicals, and their combinations with hydrogels (via both manual and microfluidic methods) were analysed. Before measurements, all samples were weighed. Phase changes and temperatures were measured with a heating/cooling rate of 10 ℃/min in the temperature range from -25 ℃ to 400 ℃. Thermograms of the samples were recorded for evaluations of drug-nanoparticle interactions with and without hydrogel matrices.

3.2.11. Structural analysis of produced liposomal nanoparticles and composite hydrogels with scanning electron microscopy (SEM)

The aim of applying SEM (Win10 FEI (Philips) XL30 microscope, FEI Company, USA) was to reveal the structures of the nanoparticles (liposomes with and without metformin) and hydrogels incorporating or not incorporating nanoparticles. The porosity and pore size of the hydrogels and the diameters of the drug-incorporated liposomes are critical parameters for controlled DDSs. The voltage

applied was 5-15 kV and the electrical current was 150 μA. Before scanning, a gold-coating process was applied for samples, and gold sputtering was done for non-conducting and poorly conducting specimens (SC7620 Mini Sputter Coater Operating Manual, Quorum Technologies, UK). Sections of the freeze-dried hydrogels and nanoparticles were removed and prepared for analysis.

3.2.12. Dissolution testing of metformin after incorporation with chitosan hydrogels

First, the dissolution medium was prepared. The medium was PBS at pH 4.5 to mimic vaginal pH. After preparation of the PBS solution, hydrogels were weighed on watch glasses to ensure that the masses of the hydrogels were the same for proper testing. Four beakers of 500 mL were then selected and labelled for dissolution testing. Each one was used for a different combination of hydrogels with liposomal nanoparticles. The first one contained chitosan hydrogel without any liposomal nanoparticles, the second contained hydrogel with 2.5 mg of lyophilized egg lecithin, the third contained hydrogel with 2.5 mg of pure metformin, and the fourth contained hydrogel with egg lecithin and metformin (1:1; w/w) (Figure 3.10). The beakers were marked and filled with 250 mL of PBS solution with a graduated cylinder at 3-min intervals. After adding the PBS solution, dissolution samples for the four beakers were taken with different 5-mL syringes at 5, 10, 15, 30, 60, 90, 120, and 240 min after test initiation at 25 ℃ (Figure 3.11). A final sample was taken at 300 min to mimic prolonged drug release with a vortex in the dissolution medium. In each time interval, samples of 1 mL were taken from each dissolution medium and transferred to Eppendorf tubes for analysis of the amount of the metformin dissolved in the hydrogels by UV-Vis spectroscopy. Following that, 1 mL of PBS solution was added to refresh the dissolution medium. Before measuring the wavelengths of the collected samples, the UV-Vis spectrophotometer (SPEKOL 1300, Analytik Jena GmbH, Germany) was checked and set at a wavelength of 234 nm because the reported wavelength of metformin in the literature is within the range of 200-400 nm and the wavelength of the standard solution of metformin HCl was recorded as 234 nm. After collection of UV-Vis spectra for the resultants , all samples were transferred to rectangular glass cells (10 mm, 3.5 mL, Agilent Technologies, USA).

The concentration released and the percentage of released metformin in the hydrogels were subsequently calculated using Eq. 3.8 and Eq. 3.9. The released amount and percent release of the drug in the hydrogels were obtained from calibration curves, which were obtained with five different concentrations of standard solution. All data were collected in triplicate (n=3) for accurate data evaluation.

$$A = \varepsilon \times m \times C \times l \tag{3.9}$$

Here, A is absorbance, ε is the molar extinction coefficient, C is the concentration, and l is the path length.

The line graph shown in Figure 3.9, which is a typical line graph with its equation, was used as calibration curve and the equation was the calibration curve equation Eq. 3.9 was used to calculations of the amount of drug released and the percentage of the drug release .Thus, (calibration curve: y=mx+n), y=absorbance(A), m= εm , slope=the molar extinction coefficient in Beer-Lambert Law Eq.3.8. Afterwards, Eq. 3.10 and Eq. 3.11, shown below, were used to evaluate the concentration of the drug and amount of drug released in dissolution media.

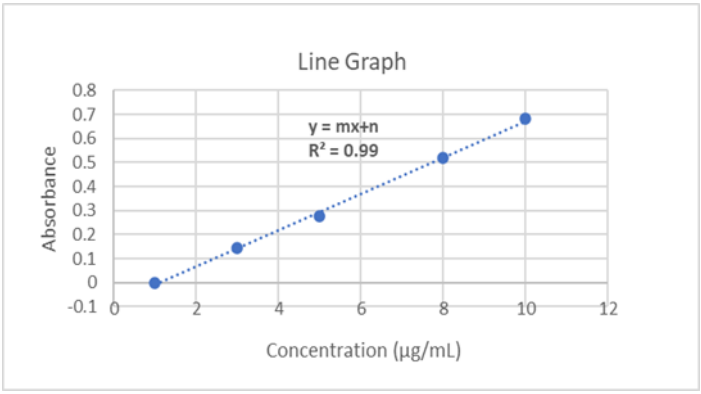

Figure 3.9: Calibration curve of absorbance vs. concentration.

$$A = \varepsilon m \times C + n \tag{3.10}$$

It is now possible to solve for C, which represents the concentration:

$$C = (A - n)/\varepsilon m \tag{3.11}$$

$$\text{Amount of drug released (mg)} = C \times D \times V_D \quad (3.12)$$

Here, C is concentration, D is the dilution factor, and V_D is the dissolution bath volume [70].

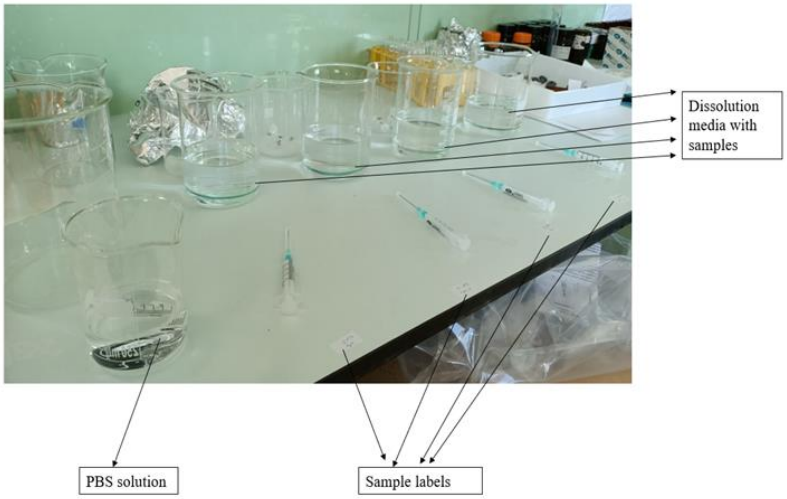

Figure 3.11: Experimental set-up for drug dissolution testing.

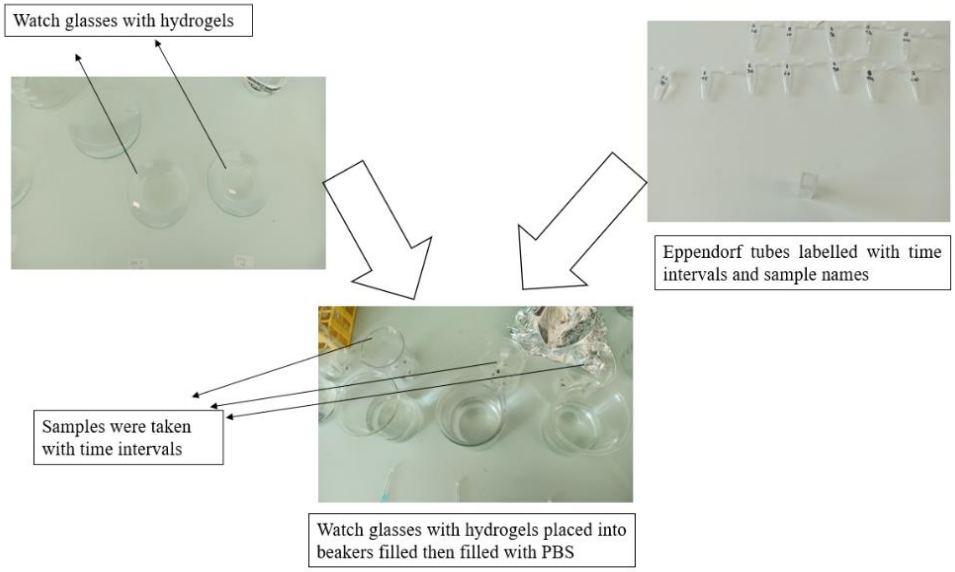

Figure 3.10: Experimental set-up for dissolution tests of hydrogel samples

4. RESULTS

4.1. Characterization studies of the produced chitosan polymer solution

Polymer solution characterization studies were conducted to evaluate the most homogeneously dispersed and transparent samples with desired pH values before and after gelation. Determination of the physicochemical properties of the chitosan solution will guide future studies of microfluidic systems. Properties such as viscosity, density, and surface tension of the polymer solution influence the droplet size and thus affect the diameters of the microbubbles Table 4.1 demonstrates the viscosity, density and surface tension of the polymer solution at room temperature.

Characterization studies were performed with different concentrations of polymer and crosslinker solutions as shown in Table 4.2 .Among the formulations, the 1% (w/v) chitosan solution and the 80% (w/w) salt solution were selected for the following experimental studies. While preparing this formulation, the impurities from the undissolved chitosan particles were minimized with proper heating and precise addition of the acid.

After the polymer solution was prepared, the chitosan polymer solution's viscosity, surface tension, and density values were measured for microfluidic experimentation, as shown in Table 4.1, one solution temperature was selected (23 ℃) because the physicochemical properties of a solution are affected by temperature. With these selected properties of the polymer solution, it was successfully passed through the microchannels of the T-shaped microfluidic device.

Table 4.1: Measured properties of 1% (w/v) chitosan polymer solution prepared (at 23℃, n=3).

Viscosity (mPa.s)	Density (g/cm^3)	Surface tension (mN/m)
90.4 ± 0.05	1.008 ± 0.002	61.96 ± 0.49

Table 4.2: Polymer solution and salt solution concentrations, pH, and solution appearances.

Trial	CS (w/v) %	Solution (w/w) %	Acetic acid (v/v) %	Initial pH	Ending pH	Solution appearance (CS solution)	Gel appearance (After adding gelling agent)
1	1.0%	60%	1%	3	4	High levels of impurities observed	Aqueous solution with impurities
2	1.5%	82%	1%	3	4	Slight impurities and bubbles observed	Slightly homogeneous transparent semi-gel solution
3	0.1%	60%	1%	3	4	Some impurities observed	Solution slightly white before addition
4	1.5%	28%	1%	6	7.5	Some impurities observed	Slightly viscous and transparent bubbly solution appeared
5	0.1%	45%	1%	3	7	High levels of impurities observed	Solution is slightly white and less viscous; no difference before adding the salt
6	1.5%	60%	1%	3	4	Slight impurities observed in transparent solution	Transparent, semi-viscous solution and bubbles observed
7	1%	80%	1%	3	4	Slight impurities observed in transparent solution	Transparent, semi-viscous solution and bubbles observed

4.2. Chemical results of FTIR spectroscopy for liposomal nanoparticles and nanocomposite hydrogels

4.2.1. FTIR results for liposomal nanoparticles with/without metformin HCl

In the literature, FTIR wavenumbers for metformin HCl are reported as 3400-3100 cm^{-1} for C=N-H [2, 71], with N-H bending (primary amine) at 1500-1580 cm^{-1} [71, 72]. C-H asymmetric bending of CH_3 at 1490-1410 cm^{-1},these peaks were found to be similar with the results obtained in studies conducted by (Zhou et al., 2018; Montané et al., 2019), C-N stretching at 1167-1064 cm^{-1}, this peak seen similar with the results obtained in the study conducted by (Zhou et al., 2014), and C-H bending at 1000-650 cm^{-1}, which were found the be similar with the results achieved in the study conducted by (Raut et al., 2013). In this experimental study, relevant wavenumbers were observed for N-H stretching at 3100 cm^{-1} for pure metformin HCl. N-H stretching was observed at 1560 cm^{-1} and 1552 cm^{-1}. C-H asymmetric bending of CH_3 was observed at 1474 cm^{-1} , 1447 cm^{-1}, and 1418 cm^{-1}, those peaks were similar with the results achieved in the study conducted by (Zhou et al., 2018). C-N stretching peaks was observed at 1167 cm^{-1}, 1077 cm^{-1}, 1061 cm^{-1}, and 1038 cm^{-1}, which were the results matching with the results achieved in studies conducted by (Raut et al., 2013; Zhou et al., 2018; Montané et al., 2019), while C-H bending was observed at 936 cm^{-1}, which had perfect match with the results achieved in the study conducted by (Raut et al., 2013).

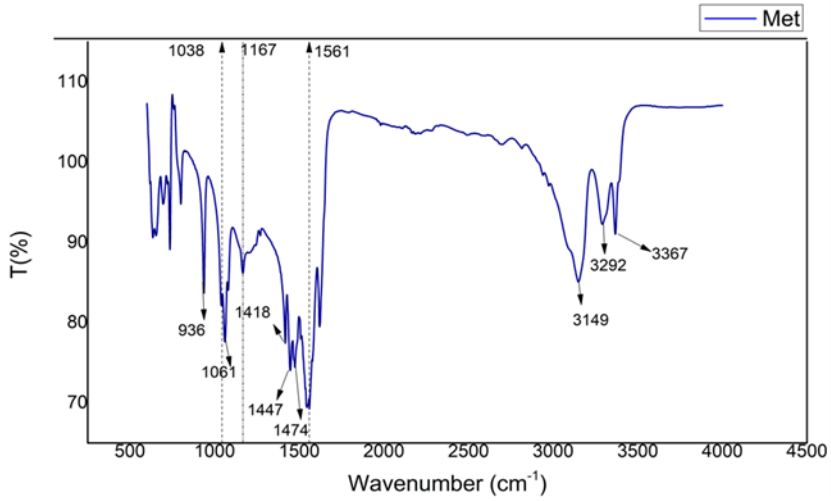

Figure 4.1: FTIR results for pure metformin; peak points are marked.

As seen in Figure 4.1 the dominant peaks of metformin were observed at 1561 cm^{-1} and 1551 cm^{-1}; these wavenumbers are associated with N-H bending groups, matching with the literature study results conducted by (Panda et al., 2018). At 1474 cm^{-1}, 1447 cm^{-1}, and 1418 cm^{-1}, peaks were observed in association with C-H asymmetric bending of the CH_3 group, were found to be similar with the results achieved in the study conducted by (Montané et al., 2019). At 1167 cm^{-1}, 1061 cm^{-1}, and 1038 cm^{-1}, peaks were observed in association with C-N stretching ,those peaks observed had a perfect match with the results achieved in the study conducted by (Kim et al., 2015). The peak observed at 936 cm^{-1} was associated with C-H bending,which is the similar results achieved of in study conducted (Raut et al., 2013). The dominant peak at 3100 cm^{-1} was associated with the N-H stretching of the C=N-H group, which was matching with the results achieved in the study conducted by (Kim et al., 2015).

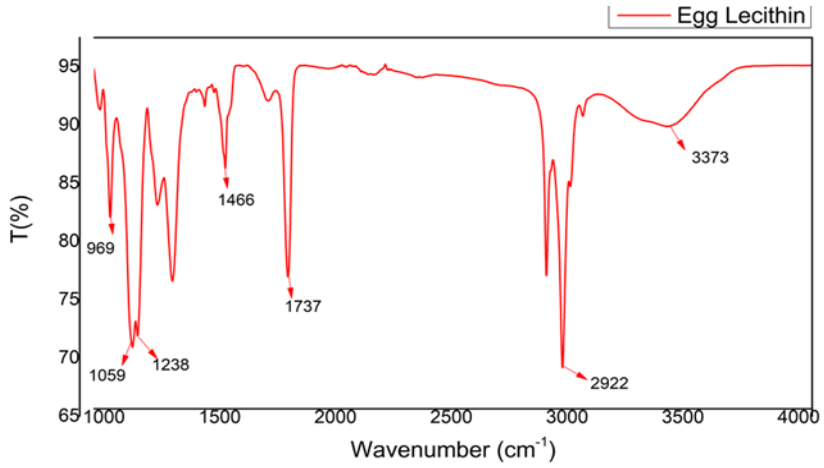

Figure 4.2: FTIR results for egg lecithin (1%) without metformin; peak points are marked.

For egg lecithin, peaks of -OH stretching were previously reported by (Latif et al., 2014) at 3200-3600 cm^{-1}. The C-H stretching vibration of the methylene group was observed at 2923-2853 cm^{-1}, the C=O stretching vibration at 1735 cm^{-1}, and a peak due to the C-H bending of the methylene group at 1466 cm^{-1}. Furthermore, peaks were reported in studies conducted by (Latif et al., 2014; Perez-Ruiz et al., 2018) 1240 cm^{-1} corresponding to the P=O stretching vibration, at 1062 cm^{-1} for the P-O-C stretching of PO_2, and at 970 cm^{-1} for the $N^+ - CH_3$ peak reported in studies conducted by (Latif et al., 2009; Tai et al., 2018). As seen in Figure 4.2, the dominant peak observed in the present work was at 969 cm^{-1} and was associated with the $N^+ - CH_3$ vibration peak of the N- $(CH_3)_3$ antisymmetric stretching group as aforementioned The peak at 1059 cm^{-1} observed may associated with the P-O-C vibration of the PO_2 symmetric stretching group, plus a CH_2 group deformation was associated with the peak at 1466 cm^{-1} for the C-H bending of the methylene group, these results were similar with the results achieved in the study conducted by (Perez-Ruiz et al., 2018). That at 1238 cm^{-1} was associated with the P=O antisymmetric stretching vibration of the PO_2 group, also the stretching vibration peak of the -OH group was observed at 3400 cm^{-1}. Finally, at 1737 cm^{-1} the vibration peak of the C=O ester stretching group was seen, while the peak for the C-H stretching vibration was

observed at 2922 cm^{-1}, those peaks observed matching with the results achieved in the study conducted by (Latif et al., 2014) [73].

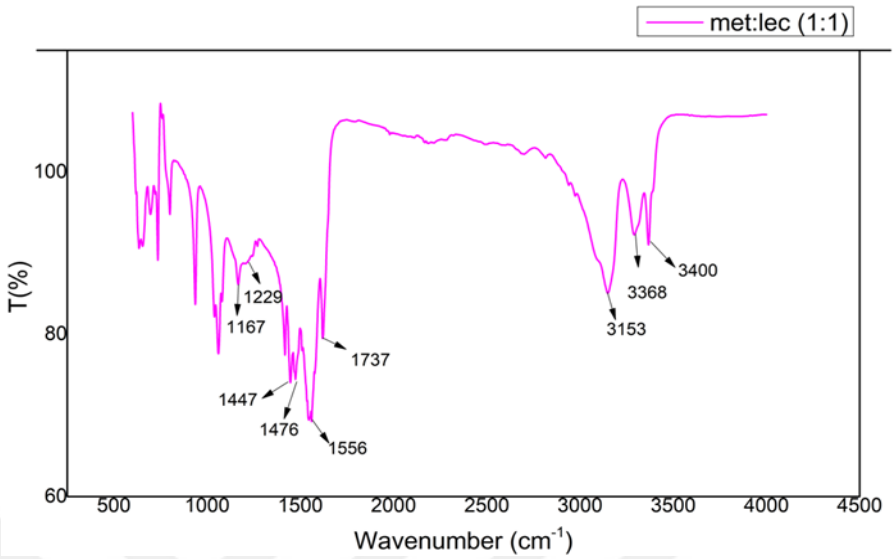

Figure 4.3: FTIR results for metformin encapsulated nanoparticles; peak points are marked.

After the incorporation of egg lecithin and metformin (Figure 4.3), the vibration of the -OH bond increased from 3373 cm^{-1} (Figure 4.2) to 3400 cm^{-1}decreases to 3368 cm^{-1} and 3153 cm^{-1}, this may be caused by the presence of the metformin's C=N-H wavenumber, which ranges from 3400-3100 cm^{-1} (Figure 4.2) and for the case of C=O the vibration of egg lecithin was kept as 1737 cm^{-1}which is the C-H bending of the methylene group, and P=O stretching vibration stretching vibration of egg the lecithin were observed at 1229 $cm^{-1}$and 1167 cm^{-1} which is associated with the antisymmetric stretching vibration of the PO_2 group, similar to the results obtained in the study conducted by (Perez-Ruiz et al., 2018). At 1556 $cm^{-1}$the peak of the N-H bending group was associated with the asymmetric bending of the CH_3 group from metformin, the peak observed matches with the results obtained in the study conducted by (Kim et al., 2015). These findings confirm that there is no chemical interaction between metformin and egg lecithin-derived liposomes (Figure 4.4).

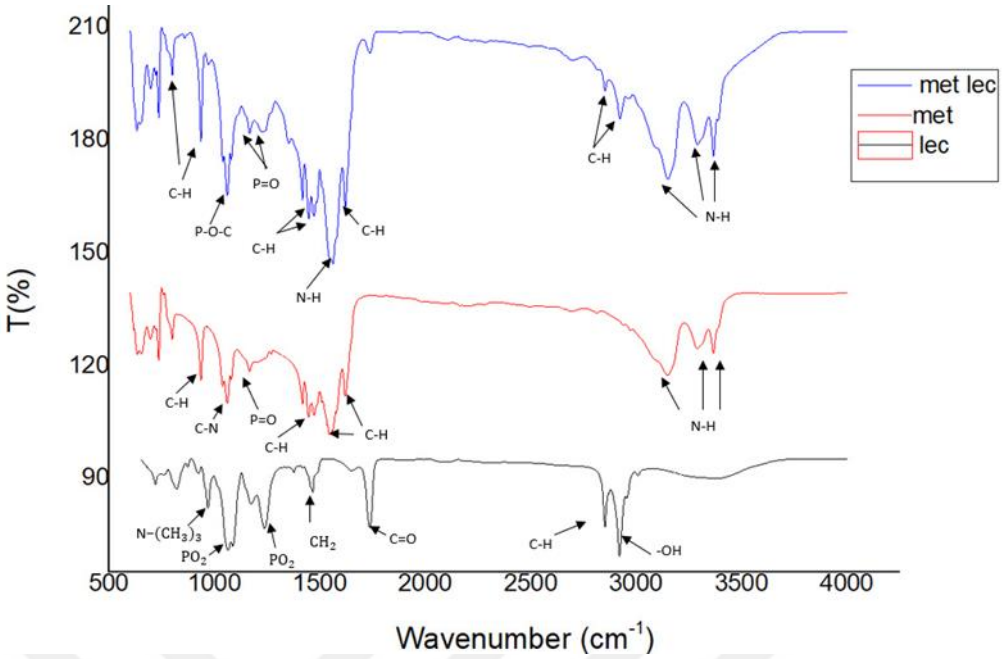

Figure 4.4: FTIR spectra of the raw materials and resultant liposomal nanoparticles (met lec: metformin and egg lecithin; met: metformin; lec: egg lecithin).

4.2.2. FTIR results for manually prepared chitosan nanocomposite hydrogel's incorporation with liposomal nanoparticles with/without metformin

In the literature, it is reported that chitosan shows characteristic peaks of the -OH asymmetrical stretching vibration at ~3425 cm^{-1}[74] and of the vibrations of C-H stretching at 3200-3500 cm^{-1} [75, 76]. Peaks are also seen (Figure 4.5) for C-H stretching at 2900-2800 cm^{-1}, similar with the results achieved in studies conducted by (Perez-Ruiz et al., 2018; De Souza Costa et al., 2009) for the amide I band at 1630-1660 cm^{-1} and for the amide II band at 1510-1570 cm^{-1}, which were similarly observed with the results of studies conducted by (De Souza Costa et al., 2009; Dimzon et al., 2015). The C-O stretching of primary alcohol groups was reported in the range of 1200-1500 cm^{-1} were similar with the results achieved in the study conducted by (Pieklarz et al., 2021) [77]. C-O stretching was noted for C-O-H at ~1160 cm^{-1} and for C-O-C at 1020 cm^{-1}, the wavenumbers seen, similar with the

results achieved in the study conducted by (Ren et al., 2017). The peak at 800-1200 cm^{-1} was associated with -O- stretching of glucosamine residues, like the results achieved in the study conducted by (Skwarczynska et al., 2018). Relevant peaks were observed with the results achieved in the study conducted by (Zhou et al., 2018) (Figure 4.5) at 3357 cm^{-1} and 3278 cm^{-1} as peaks of -OH (asymmetrical) stretching.

Peaks at 2926 cm^{-1} and 2869 cm^{-1} are associated with C-H stretching. That at 1647 cm^{-1} is associated with the C=O (amide I) group, the peaks observed similar with results achieved in the study conducted by (De Souza Costa et al., 2009). That at 1553 cm^{-1} is associated with the NH_2 (amide II) group the peak observed similar with results achieved in the study conducted by (Dimzon et al., 2015). Peaks at 1417 cm^{-1} , 1375 cm^{-1}, and 1309 cm^{-1} are associated with the -C-O stretching of the primary alcohol group of -$CH_2 - OH$ [77]. Those at 1062 cm^{-1} and 1026 cm^{-1} are associated with C-O stretching groups, namely $CH_2 - OH$ and $CH - OH$ Peaks at 896 cm^{-1}, 749 cm^{-1}, and 662 cm^{-1} are associated with the -O- of the glucosamine residue, these peaks observed similar with results achieved in the study conducted by (Skwarczynska et al., 2018) [78].

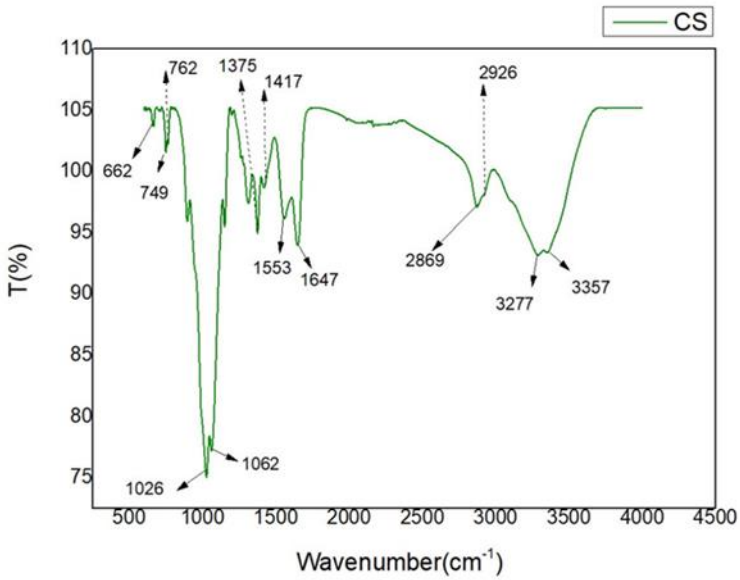

Figure 4.5: FTIR results for pure chitosan powder; peak points are marked.

For chitosan solution ionically crosslinked with β-glycerophosphate disodium salt (hydrogel), some specific peaks are given in the literature due to the phosphate groups of the gelling agent, namely the β-GP disodium salt, for aliphatic P-O-C

stretching at ~750-800 cm^{-1}, while the band at ~920 cm^{-1} corresponds to the phosphate ion -HPO_4^- group of the salt, the peaks observed which were associated with β-GP disodium salt, similar with results achieved in studies conducted by (Pieklarz et al., 2021; Ren et al., 2017). In addition, the peaks at 1050-1100 cm^{-1} correspond to the PO and PO= groups similar with results achieved in studies conducted(Perez-Ruiz et al., 2018; Maiz-Fernández et al., 2016).

In Figure 4.6, it is observed that the peaks of -OH asymmetrical stretching of the chitosan hydrogel achieved with ionic gelation with β-glycerophosphate occur at lower frequencies compared to those of pure chitosan (Figure 4.6) due to the intermolecular and intramolecular hydrogen bonds .The peaks were observed at 3236 cm^{-1} in association with the -OH (asymmetrical) band and at 2945 cm^{-1} and 2881 cm^{-1} in association with the -C-H stretching of pure chitosan, these peaks observed similar with results achieved in the study conducted by (Mansur et al., 2009).

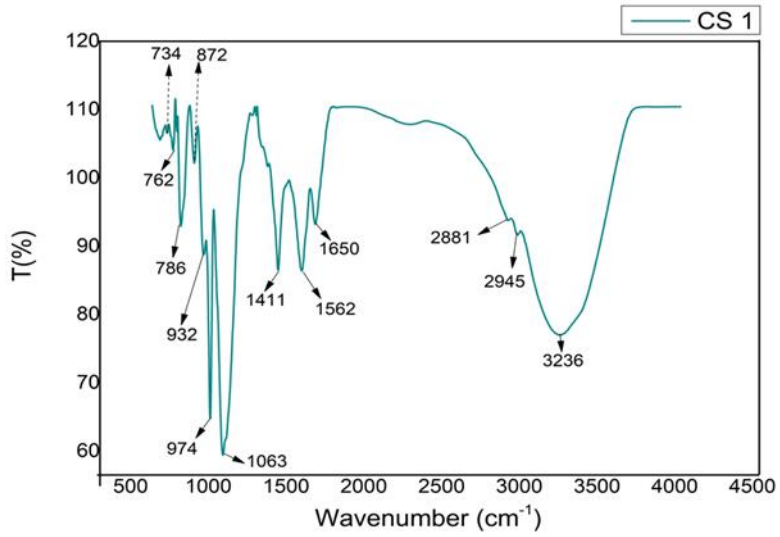

Figure 4.6: FTIR results for conventionally produced CS/β-GP hydrogel; peak points are marked

The peak at 1650 cm^{-1} for C=O (amide I) is associated with chitosan , which has the similarity with the results achieved in the study conducted by (De Souza Costa et al.,2009) That at 1562 cm^{-1} is associated with the NH_2 (amide II) group of the chitosan, the peak observed similar with the results achieved in the study conducted by (Dimzon et al., 2015). That at 1411 cm^{-1} is associated with the C-O stretching of the primary alcohol group of chitosan, -$CH_2 - OH$. The peaks at 1063 cm^{-1}, 974 cm^{-1}, 932 cm^{-1}, and 872 cm^{-1} are associated with the characteristic saccharide

structure of chitosan with oxygen bridge bonds of C-O-C and CH_3COH groups. The peaks at 786 cm^{-1}, 762 cm^{-1}, and 734 cm^{-1} are associated with aliphatic P-O-C stretching, as seen in Figure 4.6, those peaks observed, had perfect match with the results achieved in the study conducted by (Piekalrz et al., 2021). The peak at 1063 cm^{-1} is associated with the PO and PO= groups of β-glycerophosphate, this peak observed, similar with the results achieved in the study conducted by (Maiz-Fernández et al., 2016).

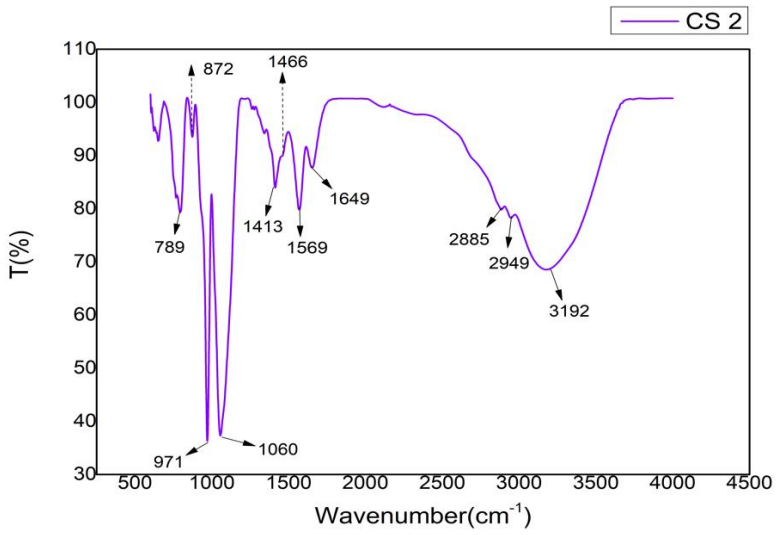

Figure 4.7: FTIR results for CS/β-GP hydrogel with empty liposomal nanoparticles; peak points are marked.

In the FTIR spectrum of the hydrogel with empty egg lecithin nanoparticles (Figure 4.7), the characteristic peaks of chitosan and egg lecithin are observed. At 3192 cm^{-1}, the vibration peak is associated with chitosan's -OH asymmetrical stretching vibration, the peak observed similar with the results achieved in the study conducted by (Zhou et al., 2018). The peaks at 2885 cm^{-1} and 2949 cm^{-1} can also be considered as C-H stretching peaks of pure chitosan, those peaks observed similar with the results achieved in the study conducted by (De Souza Costa et al., 2009). The peak at 1649 cm^{-1} is associated with the amide I band vibration frequency of the chitosan. The peak at 1569 cm^{-1} is associated with the amide II band frequency, the peak observed similar with the results achieved in the study conducted by (Dimzon et al., 2015). That at 1466 cm^{-1} is associated with the C-H bending of the methylene group of egg lecithin, the peak observed similar with the results achieved in the study conducted by (Latif et al., 2014). The peak at 1060 $cm^{-1}$is associated

with the PO and PO= groups of the β-glycerophosphate crosslinker, those peaks observed, similar with the results achieved in the study conducted by (Maiz-Fernández et al., 2016). The vibration peak of 789 cm^{-1} is associated with the aliphatic P-O-C stretching of β-glycerophosphate. The peak at 971cm^{-1} may indicate the characteristic PO_4^{2-}group associated with the presence of β-glycerophosphate, those peaks observed were similar with the results obtained in the study (Pieklarz et al., 2021).

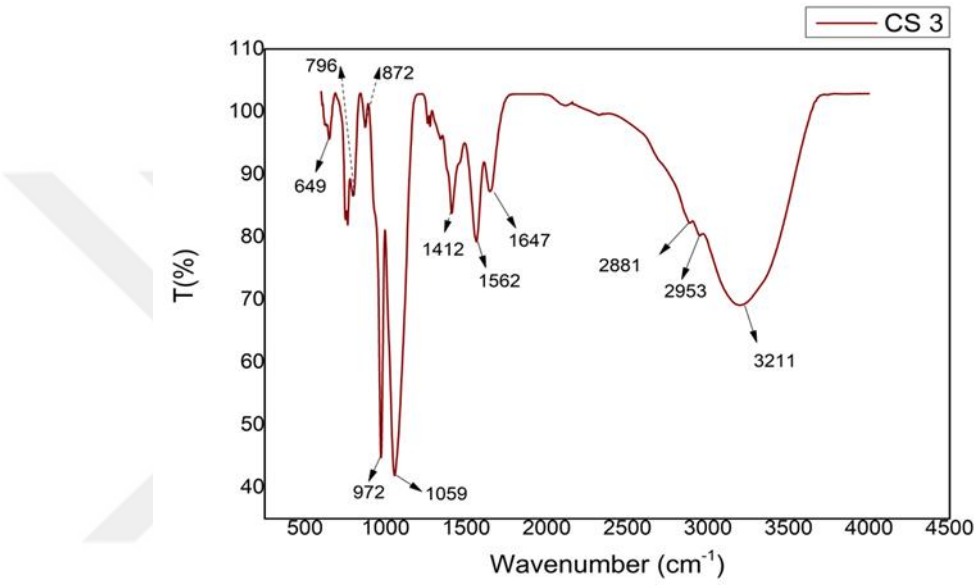

Figure 4.8: FTIR results for CS/β-GP hydrogel with metformin; peak points are marked.

For the hydrogel with metformin (Figure 4.8), the peak at 1412 cm^{-1} may be associated with the C-H asymmetric bending of both pure metformin and chitosan, the results were found to be similar with the result achieved in studies conducted by (Kim et al., 2015; Pieklarz et al., 2021). For the hydrogel with freeze-dried metformin encapsulated liposomal nanoparticles the peak of the aliphatic chitosan ring previously observed at 2953 cm^{-1} had a lower value of 2934 cm^{-1} (Figure 4.8), and this was the lowest peak for this vibration due to the addition of nanoparticles with the combination of drug and liposomes in the hydrogel matrix. The peak at 1562 cm^{-1} is associated with the NH_2 (amide II) group of chitosan, the peak observed is similar with the results achieved in the study conducted by (Dimzon et al., 2015). The peak at 1059 cm^{-1} is associated with the P-O-C stretching group of the crosslinker (β-GP), that at 972 cm^{-1} is associated with the $-HPO_4^-$ group, and that at 872

cm^{-1} is associated with either the P-O-C aliphatic stretching group of the β-GP crosslinker, these peaks were observed parallel with the results achieved in the study conducted by (Maiz-Fernández et al., 2016) or the oxygen bridge bonds of the C-O-C and CH_3COH groups of chitosan, the oxygen bridge bond observed similar with the results achieved in the study conducted by (Pieklarz et al., 2021). Also, the peaks at 1200-800 cm^{-1} that may be associated with chitosan's characteristic saccharide structure are seen at 1059 cm^{-1}, 972 cm^{-1}, and 872 cm^{-1}, is similar with the results achieved in the study (Pieklarz et al., 2021).

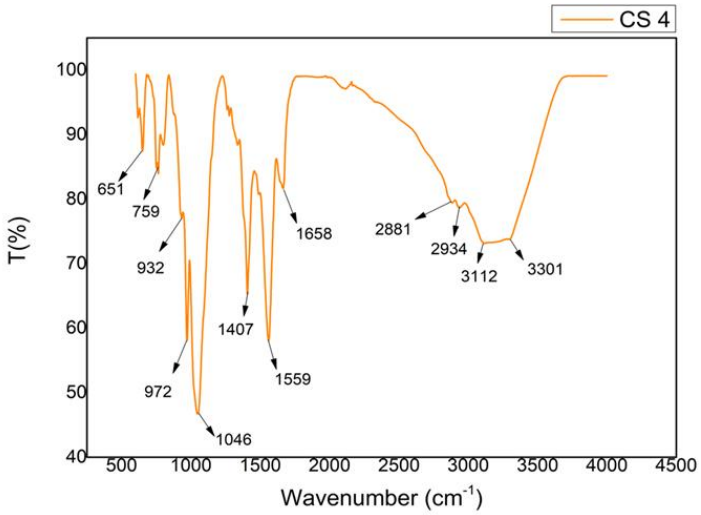

Figure 4.9: FTIR spectra of CS/β-GP hydrogel with metformin encapsulated liposomal nanoparticles; peak points are marked.

Regarding the nanocomposite hydrogel with incorporation of metformin encapsulated liposomal nanoparticles, peaks were observed for the -OH (asymmetrical) band at 3300 cm^{-1} and 3112 cm^{-1} and the peak at 1658 cm^{-1} is associated with the C=O (amide I) group of chitosan, which has the similarity with the results achieved in the study conducted by (De Souza Costa et al., 2009). The peaks at 2934 cm^{-1} and 2881 cm^{-1}, related to the C-H stretching group, which were similar with the results obtained in the study conducted by (Mansur et al., 2009) (Figure 4.9). In addition, that at 1559 cm^{-1} may be related to the N-H bending group associated with the asymmetric bending of the CH_3 group of metformin, the N-H bending of the metformin demonstrated a similar peak with the results achieved of the study conducted by (Kim et al., 2015). That at 1407 cm^{-1} is associated with the CH_2 deformation of the methylene groups of egg lecithin, those peaks were found to

be matching with the results achieved in the study conducted by (Latif et al., 2014). The peak at 932 cm^{-1} is associated with the -HPO_4^- group, just like the results in the study conducted by (Maiz-Fernández et al., 2020), and those at 759 cm^{-1} and 651 cm^{-1} are associated with P-O-C groups from the β-glycerophosphate salt, in which the peaks were observed similar with the results achieved in the study conducted by (Pieklarz et al., 2021) (Figure 4.10).

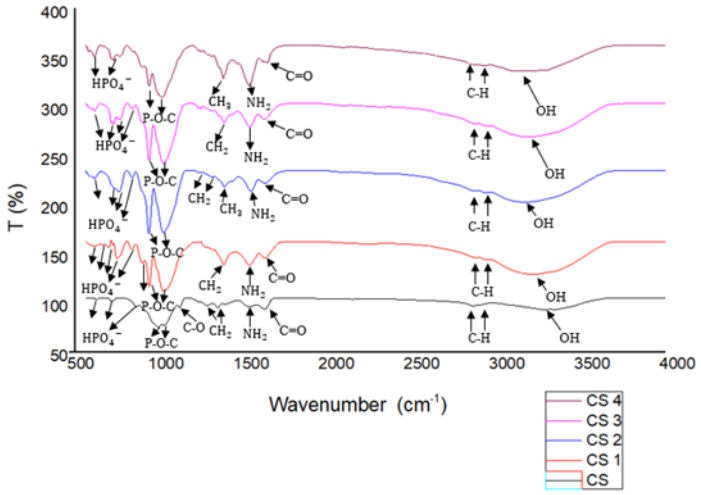

Figure 4.10: FTIR spectra of CS, pure chitosan powder; CS 1, CS/β-GP hydrogel; CS 2, CS/β-GP hydrogel/liposomal particles; CS 3, CS/β-GP hydrogel/metformin; CS 4, CS/β-GP hydrogel/metformin encapsulated liposomal nanoparticles.

Overall, the changes seen in the peaks of the FTIR spectrum for CS 4 are associated with the liposomal nanoparticles in the polymer matrix. There is no considerable difference between the peaks of the chitosan hydrogel or the combinations with the drug and drug-loaded liposomes (Figure 4.9). All peaks were observed in the fingerprint region of the IR spectra, demonstrating that there is no possible incompatibility among metformin, metformin encapsulated liposomal nanoparticles, and the hydrogel (CS/β-GP). FTIR analysis of the freeze-dried hydrogel (CS/β-GP) with the additions of different nanoparticles (freeze-dried egg lecithin with and without metformin, pure metformin) was also conducted and relevant peaks were found according to the literature (Figure 4.10). The characteristic peaks of both chitosan and β-glycerophosphate were observed in the spectra of the

gel, similar with the results achieved in the study conducted by (Maiz-Fernández et al., 2020).

4.2.3. FTIR results for microfluidically prepared hydrogels with different formulations

Regarding the FTIR spectra of the hydrogels produced via microfluidics (M-CS 1, M-CS-2, M-CS 3, and M-CS 4) seen in Figure 4. 11, relevant wavenumbers of chitosan were observed for all of them, as explained in Chapter 4.1.2. The characteristic peaks of polysaccharide belong to the -OH group (Figure 4. 11) and are seen at 3165-3179 cm^{-1}. The characteristic peaks determined seen in had perfect match with the results achieved in the study conducted by (De Souza Costa et al., 2009).

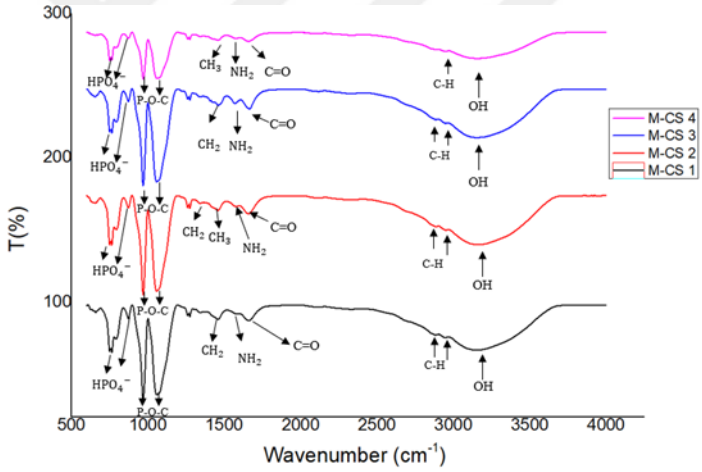

Figure 4. 11: FTIR spectra of M-CS 1, microfluidically prepared CS/β-GP hydrogel; M-CS 2, microfluidically prepared CS/β-GP hydrogel/liposomal particles; M-CS 3, microfluidically prepared CS/β-GP hydrogel/metformin; M-CS 4, microfluidically prepared CS/β-GP hydrogel/metformin encapsulated liposomal nanoparticles.

This peak slightly differs for each hydrogel due to different combinations of nanoparticles and the active ingredient -OH. The lowest peak among the hydrogels (M-CS 1, M-CS 2, M-CS 3, M-CS 4) belonged to M-CS 4 and was observed at 3173 cm^{-1}. This decrease can be explained by the intermolecular and intramolecular hydrogen bonds, were similar with the results achieved in the study conducted by (De

Souza Costa et al., 2009). The ionically crosslinked microfluidically prepared hydrogel (CS/β-GP) has dominant peaks. In Figure 4.12, the dominant peak at 3169 cm^{-1} is associated with the -OH (asymmetrical) group while those at 2945 cm^{-1} and 2877 cm^{-1} are related to the -C-H stretching group ,parallel to the results achieved in the study conducted by (Perez-Ruiz et al., 2018). The peak at 1660 cm^{-1} is related to the presence of the C=O (amide I) group, and that at 1459 cm^{-1} is associated with the NH_2 (amide II) group, related to the results obtained from the study conducted by (Pieklarz et al., 2021).

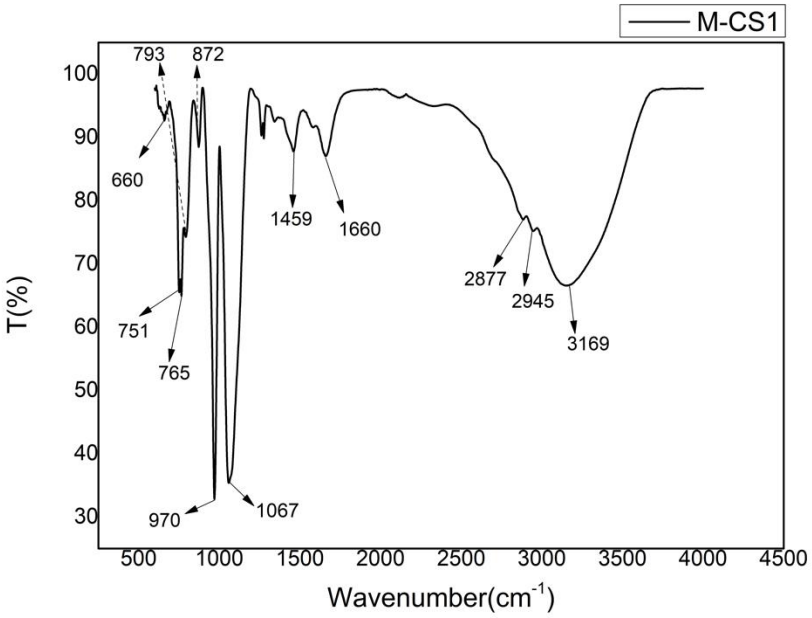

Figure 4.12: FTIR results for microfluidically prepared CS/β-GP hydrogel; peak points are marked.

The peaks at 1275 cm^{-1} and 1261 cm^{-1} correspond to the -C-O stretching of primary alcohol group -$CH_2 - OH$ in the presence of chitosan. Other peaks that were observed are related to the crosslinker (β-GP); specifically, that at 1067 cm^{-1} is associated with the P-O and -P=O groups, that at 970 cm^{-1} corresponds to the P-OH group, and that at 872-751 cm^{-1} is related to the aliphatic stretching of the P-O-C group (Figure 4.12). Those peaks were mentioned were found to be similar with the results obtained in the study conducted by (Pieklarz et al., 2021).

For the microfluidically prepared hydrogel with liposomal nanoparticles without metformin, the dominant peaks of chitosan are presented in Figure 4.13. The

peak at 3180 cm^{-1} is associated with the OH (asymmetrical) group, like the FTIR results achieved in the study conducted by (De Souza Costa et al., 2014). Those at 2941 cm^{-1} and 2885 cm^{-1} correspond to the -C-H stretching group, the peaks observed similar to with FTIR result achieved in the study conducted by (Perez-Ruiz et al., 2018). C=O (amide I) group peaks were observed similar with FTIR results achieved in the study conducted by (Pieklarz et al., 2021) which were at 1658 cm^{-1} and 1574 cm^{-1}. That at 1459 cm^{-1} is associated with NH_2 (amide II). Also the ones at 1276 cm^{-1} and 1261 cm^{-1} are associated with the -C-O stretching of the primary alcohol group of chitosan, $-CH_2-OH$. The peak observed at 1058 cm^{-1} is associated with the P-O-C stretching vibration of egg lecithin ,had matched with the results achieved in the study conducted by (Perez-Ruiz et al., 2018). The peaks related to the crosslinker (β-GP) were observed at 873 cm^{-1}, 794 cm^{-1}, 765 cm^{-1}, and 751 cm^{-1} and were attributed to the aliphatic stretching of the P-O-C group. The peak at 970 cm^{-1} is associated with the $-HPO_4^-$ phosphate ion group, the crosslinker effect seen, is similar with results achieved in the study which is conducted by (Pieklarz et al, 2021).

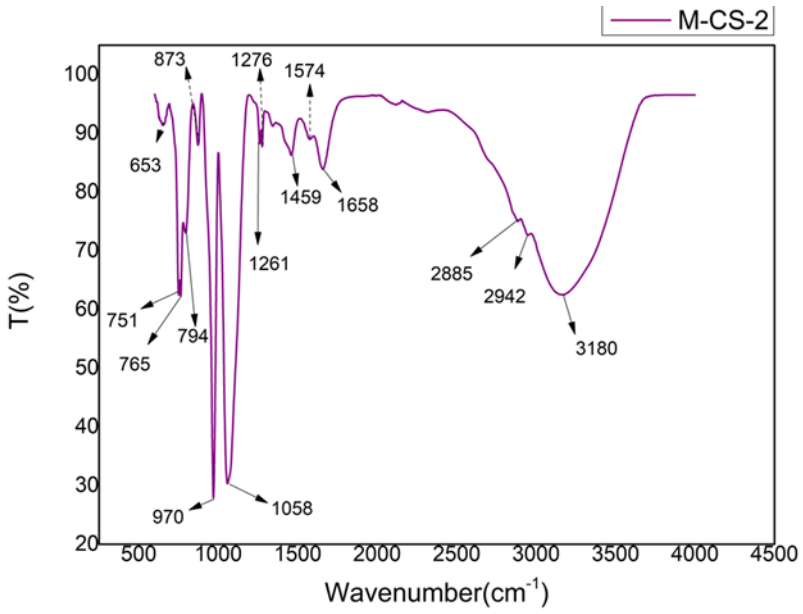

Figure 4.13: FTIR results for microfluidically prepared CS/β-GP hydrogel with liposomal particles; peak points are marked.

In Figure 4.14, for the microfluidically prepared hydrogel with pure metformin, a peak is seen at 3178 cm^{-1}, associated with the -OH (asymmetrical) group of chitosan, which is similar to the results in the study conducted by (De Souza Costa et al., 2009). Those at 2949 cm^{-1} and 2881 cm^{-1} are associated with -C-H stretching groups, match with the results achieved in the study conducted by (Perez-Ruiz et al., 2018). At 1664 cm^{-1}, the peak is associated with the C=O (amide I) group and at 1459 cm^{-1} it is associated with the NH_2 (amide II) group, which is similar with the results obtained from the FTIR spectra in the study conducted by (Dimzon et al., 2015) which may be related to the C-N stretching of metformin. The peak at 1572 cm^{-1} is also associated with the C-N stretching of metformin, which were similar with the result in the study conducted by (Kim et al., 2015). The peaks at 1261 cm^{-1} and 1276 cm^{-1} are associated with the primary alcohol groups of chitosan. The characteristic absorption peaks of β-glycerophosphate disodium salt were also observed. In Figure 4.12, the peaks at 873 cm^{-1}, 796 cm^{-1}, 766 cm^{-1}, and 751 cm^{-1} are associated with the aliphatic stretching of the P-O-C groups of β-GP and the peaks at 873 cm^{-1}, 1066 cm^{-1}, and 970 cm^{-1} may be associated with the characteristic saccharide peaks of chitosan. Finally, the peak at 970 cm^{-1} may indicate the $-HPO_4^-$ (phosphate ion) of the crosslinker, the peaks mentioned, were similar with the results achieved in the study conducted by (Pieklarz et al., 2021) .

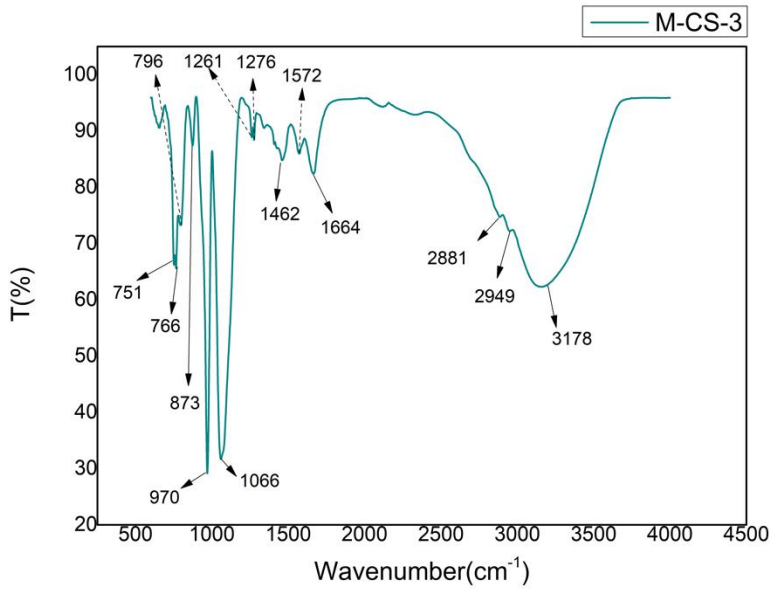

Figure 4.14: FTIR results for microfluidically prepared CS/β-GP hydrogel with metformin; peak points are marked.

The results of the FTIR analysis of the nanocomposite hydrogel with metformin encapsulated liposomal nanoparticles are shown below (Figure 4.15). The dominant peaks of the functional groups were detected. For chitosan, the peak of the -OH (asymmetrical) group was observed at 3173 cm^{-1}, in which similar with the results in the study conducted by (De Souza Costa et al., 2014). Peaks at 2949 cm^{-1} and 2885 cm^{-1} were associated with the presence of the -C-H stretching groups of chitosan, those peaks were similarly observed in the results achieved in the study conducted by (Perez-Ruiz et al., 2018). That at 1659 cm^{-1} is a characteristic peak of chitosan associated with the C=O (amide I) group. The peaks at 1276 cm^{-1} and 1258 cm^{-1} correspond to chitosan's -C-O stretching of the primary alcohol group, namely $-CH_2-OH$, those peaks observed, had a perfect match with the results achieved in the study conducted by (Pieklarz et al., 2021). That at 1458 cm^{-1} is associated with the C-H bending of the methylene group in egg lecithin ,which were similar results with the results achieved in the study conducted by (Latif et al., 2014). There is no characteristic peak of metformin, confirming that the metformin is encapsulated in the liposomal nanoparticles. The characteristic peaks of the β-GP salt were also observed; that at 1060 cm^{-1} can be associated with P-O and P=O groups and that at 970 cm^{-1} is associated with HPO_4^- (phosphate ion). Those at 872 cm^{-1},

792 cm^{-1}, and 766-749 cm^{-1} are associated with the aliphatic stretching of the P-O-C group ,those results parallel with the results achieved in the study conducted by (Pieklarz et al., 2021).

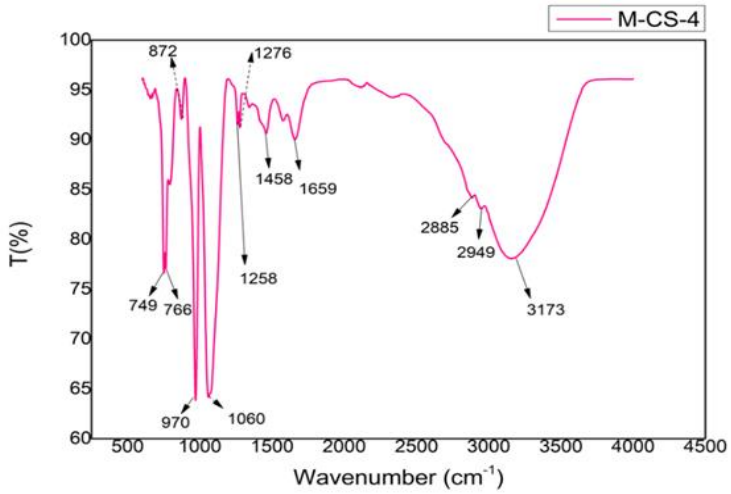

Figure 4.15: FTIR results for microfluidically prepared CS/β-GP hydrogel with metformin encapsulated nanoparticles; peak points are marked.

4.3. Structural characterization results of liposomal nanoparticles and nanocomposite hydrogels with/without metformin

4.3.1. Optical microscopy results of microbubble characterization for liposomal nanoparticles and nanocomposite hydrogels

From the images obtained with an optical microscope, uniform, monodisperse chitosan microbubbles were observed (Figure 4.16). Hence, the desired uniformity was achieved. Uniformity is a critical parameter for hydrogel DDSs, not only for generating homogeneous hydrogel platforms but also for facilitating manipulation of the dosage of the drug [20]. The obtained bubbles maintained their shapes for 1 h. This confirmed that the microbubbles initially remained monodisperse and stable; however, as time passed, the bubbles no longer kept their stability in air. The size distribution of the chitosan microbubbles is shown in Figure 4.17. The average size of the microbubbles was found to be 144.5 μm and the PDI value was 18.8%.

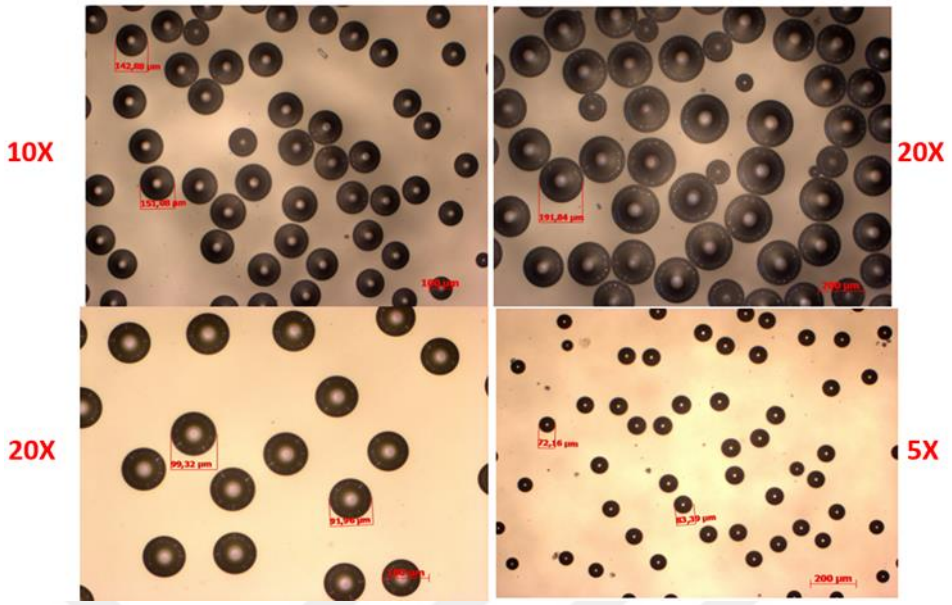

Figure 4.16: Optical microscopy images of monodispersed chitosan group of microbubbles via T-junction microfluidic device with different magnifications.

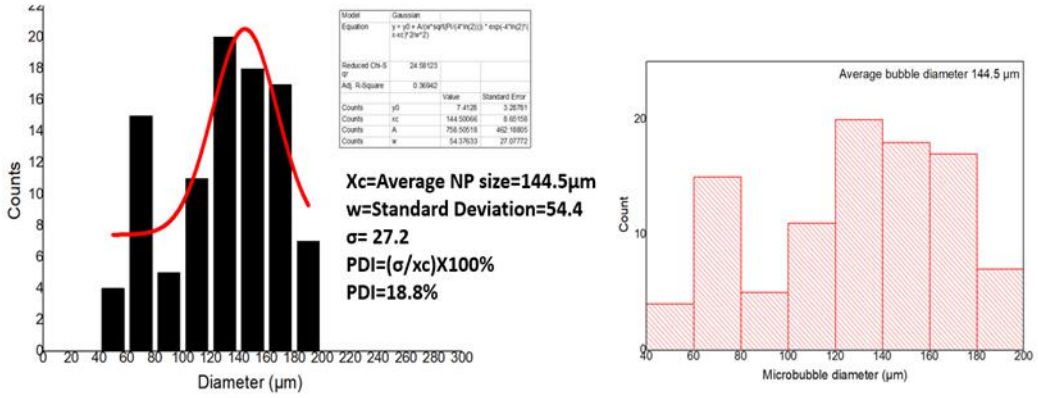

Figure 4.17: Size distribution of chitosan microbubbles with an average bubble size, obtained.

4.3.2. Scanning Electron Microscopy (SEM)

Freeze-dried egg lecithin, pure metformin, and egg lecithin incorporated with metformin were sectioned for SEM imaging. This procedure was also applied for the

chitosan hydrogels with and without nanoparticles, which had been produced by means of both manual and microfluidic methods.

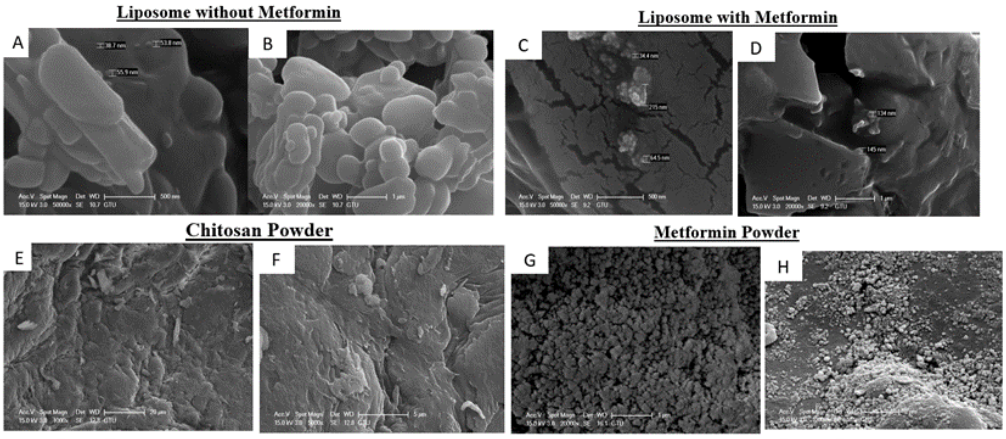

Figure 4.18: Scanning electron micrographs of liposomes derived from egg lecithin (A, B), metformin encapsulated liposomal nanoparticles (C, D), pure chitosan powder (E, F), and pure metformin drug powder (G, H).

Figure 4.18, empty egg lecithin liposomes are seen to have smooth and spherical surfaces. After incorporation with metformin, the freeze-dried samples demonstrated a spherical shape and the size of the liposome vesicles was increased with the addition of the drug.

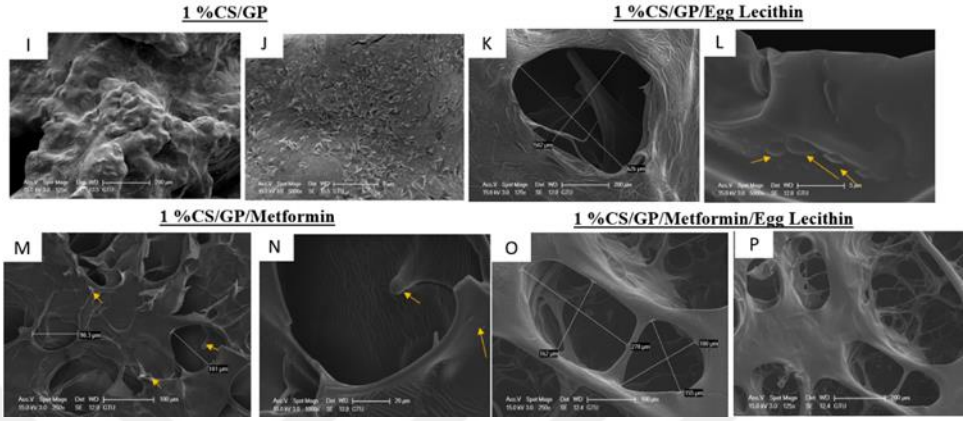

Figure 4.19: Scanning electron micrographs of manually prepared 1% CS/GP hydrogel (I, J), 1% CS/GP/liposomal nanoparticles (K, L), 1% CS/GP/metformin (M, N), and 1% CS/GP/metformin encapsulated nanoparticles (O, P).

SEM images also revealed the morphology of the conventionally prepared hydrogel system (Figure 4.19). The porous nature of the freeze-dried samples of 1% chitosan/ β-glycerophosphate disodium salt hydrogel is shown (K, M, O, P).

In addition, embedded nanoparticles (lecithin with/ without metformin, pure metformin) were seen in the hydrogel matrix (Figure 4.19, L, M, N). SEM images of hydrogel platforms prepared by the microfluidic method also revealed a porous surface morphology with micron-sized pores. The size of these pores was considerably smaller compared to those of the conventionally prepared hydrogels. This reduction in size was achieved with the careful addition of the crosslinker (β-GP) and chitosan microbubbles during gelation. Moreover, the cavities of the manually prepared hydrogel systems were not regular (Figure 4.19, O, P), in contrast to the hydrogels prepared by the microfluidic method (Figure 4.20, R, Q). The cavities of manually prepared hydrogels were observed as foliate structures (Figure 4.19, M, N), while microfluidically generated hydrogels had a sponge-like

morphology (Figure 4.20). The PDI values of the prepared hydrogels were also calculated using the ImageJ and Origin Lab software programs.

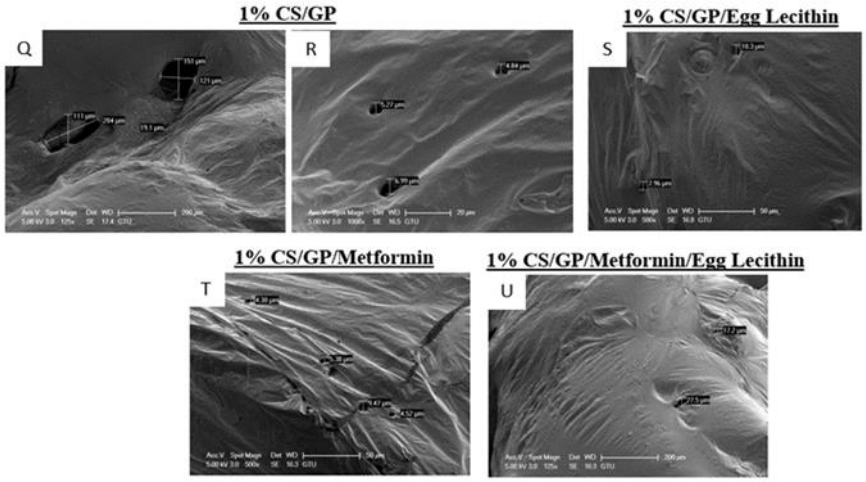

Figure 4.20: Scanning electron micrographs of microfluidically prepared 1% CS/GP hydrogel (Q, R), 1% CS/GP/liposomal nanoparticles(S), 1% CS/GP/metformin (T), and 1% CS/GP/liposomal metformin (U).

As seen in Figure 4.21, the manually prepared hydrogels have an average pore size of 150 μm, whereas hydrogels prepared by the microfluidic method have an average pore size of 6.8 μm. It can be concluded that the pore size of the crosslinked hydrogels is drastically decreased by using the microfluidic method. Accordingly, the PDI values of the pores were calculated. They were found to be 20% for the manually prepared hydrogels (empty/ nanocomposite) and 42% for the microfluidically prepared hydrogels (empty /nanocomposite). Thus, the monodispersity of the manually prepared hydrogels was found to be higher than that of the microfluidically prepared hydrogels. This could be explained by several factors; solution properties (viscosity and surface tension) and gas/ flow rate ratio [79, 80].

Although the microfluidic system downsized the pore size diameter of the hydrogels (see Figure 4.21) and also monodispersed microbubbles generated, the pore size of the microfluidically prepared hydrogel platforms were found to be more polydispersed compared to the conventionally made hydrogels. This was earlier explained by (Parhizkar et al., 2014), that the cumulation of the microbubbles will, create pressure on bubbles located on the lower layers while collecting them, and will lead to a broad range of pore size distribution. [81].

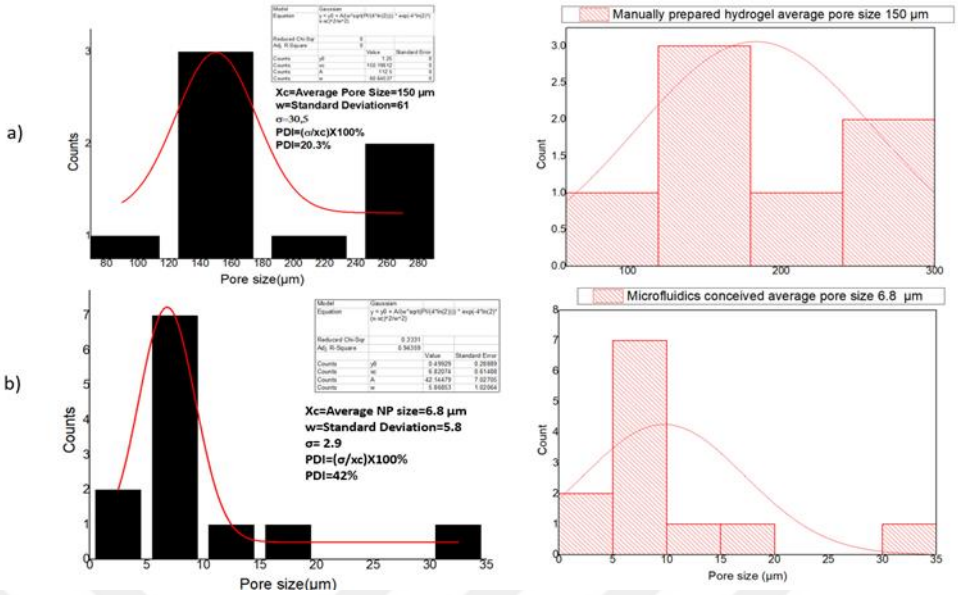

Figure 4.21: Average pore size distributions with PDI values for a) manually prepared nanocomposite hydrogels with/without nanoparticles and b) microfluidically prepared nanocomposite hydrogels with empty hydrogels with/ without nanoparticles.

4.4. Thermal analysis results by differential scanning calorimetry for liposomal nanoparticles and nanocomposite hydrogels

Differential scanning calorimetry (DSC) was used for the characterization of the thermal behaviour of the materials. DSC thermograms provide data about drug-polymer interactions via information about peaks, such as the appearance/ disappearance of peaks or melting points. In this experimental study, freeze-dried samples (both nanoparticles and hydrogel that are incorporated with nanoparticles) were used for DSC analysis. As seen in Figure 4.22, the DSC thermal analysis spectra , which has the sharp endothermic peak of pure metformin (met), was observed at 232 ℃, corresponding to its melting point. The thermogram of β-glycerophosphate demonstrated a sharp endothermic peak at 303 ℃. For the freeze-dried metformin and egg lecithin (met lec (1:1)), the endothermic peak was seen at 224 ℃.

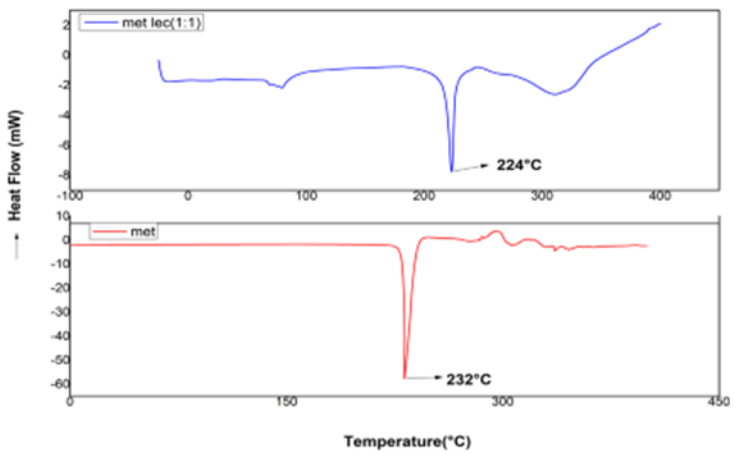

Figure 4.22: DSC analysis of pure metformin (met) and metformin incorporated with egg lecithin (met lec (1:1)).

This peak confirms that there was an interaction between metformin and egg lecithin, or, in other words, between the drug and the liposome, which demonstrates the possibility of drug loading on the liposomes. For the pure chitosan powder (Figure 4.23), two peaks were observed at 97 ℃ (endothermic) and 300 ℃ (exothermic). Those peaks are associated with both water loss and polymer degradation, which includes saccharide ring dehydration, depolymerization, and acetylated decomposition of the chitosan unit. For crosslinked chitosan hydrogels CS 1, CS 2,

CS 3, and CS 4 (Figure 4.24), the chitosan hydrogel without nanoparticles (met/met lec/lec) demonstrated three endothermic peaks at 67 ℃, 128 ℃, and 243 ℃.

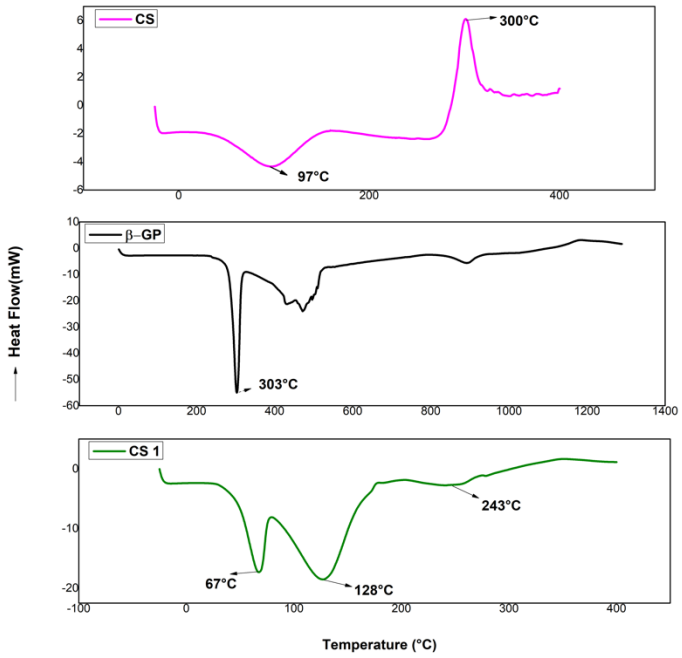

Figure 4.23: DSC analysis of pure chitosan powders (CS), pure beta glycerophosphate (β-GP), and manually prepared CS/β-GP hydrogel (CS 1).

Compared to the pure chitosan (CS), additional peaks and the disappearance of the endothermic peak were observed for CS 1 due to the interactions of the crosslinker and the chitosan polymer. For the hydrogel loaded with only egg lecithin (CS 2), endothermic peaks were observed at 113 ℃ and 243 ℃, and these changes in the thermal peaks were related to the interactions between empty liposomes. For CS 3 and CS 4, slight changes were observed for the endothermic peaks at 100 ℃ (CS 3) and 102 ℃ (CS 4). This may indicate interactions between the hydrogel and other moieties. In addition, an endothermic peak of CS 4 was observed at 242 ℃ due to the presence of egg lecithin, and this value was much closer to the endothermic peak of CS 2. The sharp peak of metformin, which was found at 231 ℃, was not observed

for CS 3 and CS (Figure 4.24). This indicates that the drug was uniformly dispersed in an amorphous state with the CS/β-GP hydrogel matrix (Figure 4.25).

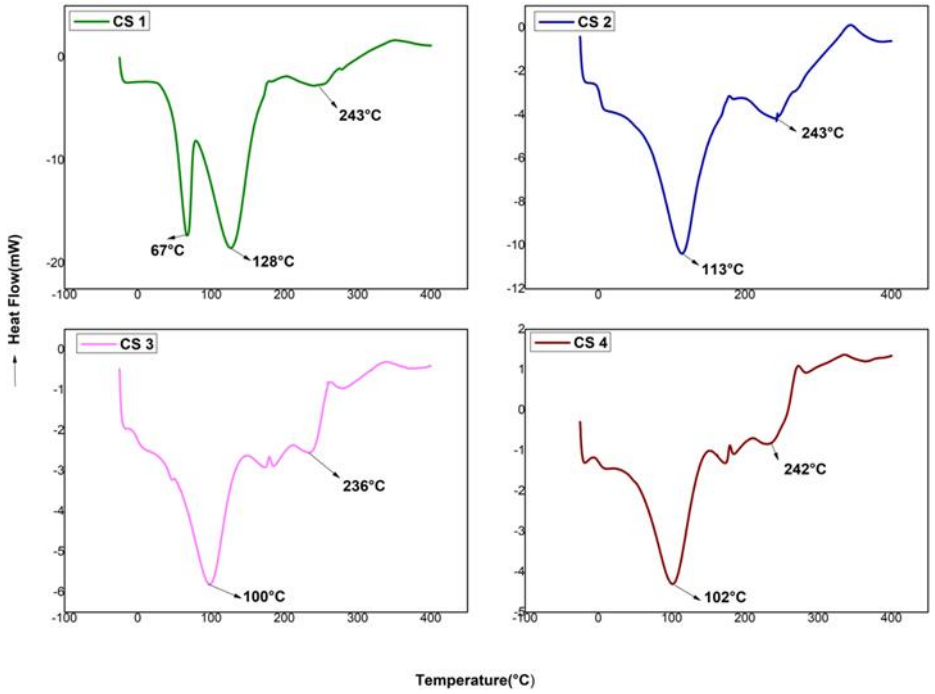

Figure 4.24: DSC analysis of manually produced hydrogels: CS 1, manually prepared CS/β-GP hydrogel; CS 2, manually prepared CS/β-GP hydrogel with liposomal particles; CS 3, manually prepared CS/β-GP hydrogel with pure drug; CS 4, manually prepared CS/β-GP hydrogel incorporated with metformin encapsulated liposomal nanoparticles.

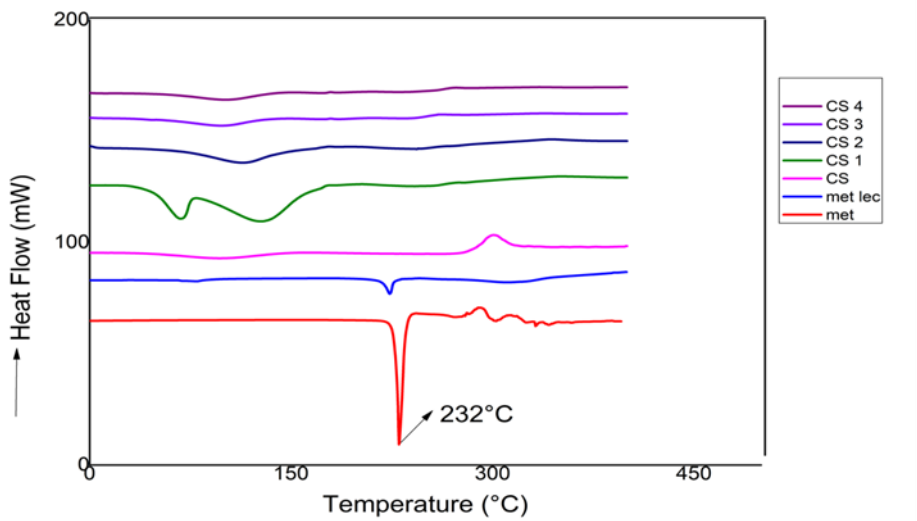

Figure 4.25: Metformin drug (met), metformin incorporated with egg lecithin liposomes (met lec), chitosan powder (CS), microfluidically prepared CS/β-GP hydrogel (M-CS 1), microfluidically prepared CS/β-GP hydrogel with egg lecithin (M-CS 2), microfluidically prepared CS/β-GP hydrogel with metformin (M-CS 3), microfluidically prepared CS/β-GP hydrogel with metformin encapsulated nanoparticles (M-CS 4).

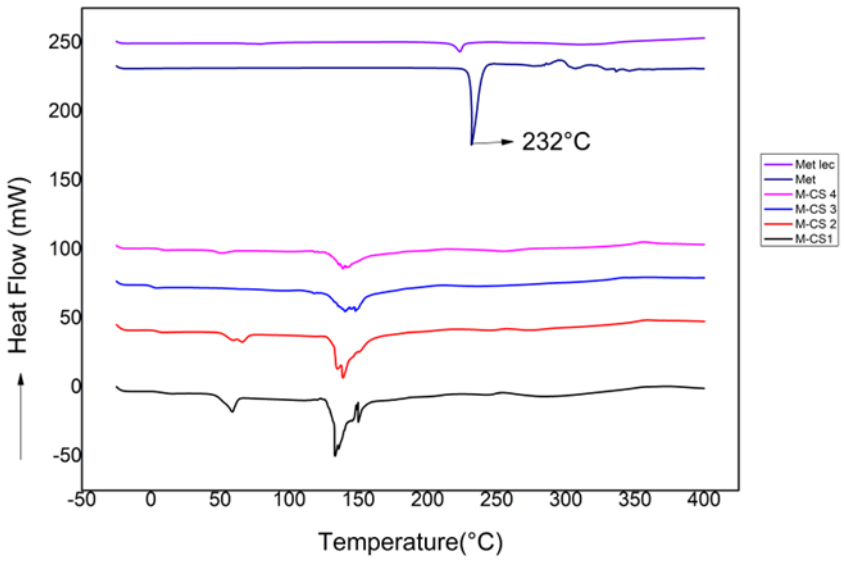

Figure 4.26: Metformin drug (met), metformin incorporated with egg lecithin liposomes (met lec), chitosan powder (CS), microfluidically prepared CS/β-GP hydrogel (M-CS 1), microfluidically prepared CS/β-GP hydrogel with liposomal nanoparticles (M-CS 2), microfluidically prepared CS/β-GP hydrogel with metformin (M-CS 3), microfluidically prepared CS/β-GP hydrogel with egg metformin encapsulated nanopartciles (M-CS 4).

A further thermogram (Figure 4.26) presents the findings for the hydrogels produced by microfluidics (M-CS 1, M-CS 2, M-CS 3, and M-CS 4). Slight changes are observed when we compare each of them. Similarly, to the conventionally prepared chitosan hydrogel (CS 1), the microfluidically prepared hydrogel (M-CS 1) exhibited three endothermic peaks as observed in the thermograms (Figure 4.27). However, the endothermic peak values of M-CS 1 are much lower than those of CS 1. This may indicate the thermal decomposition of the hydrogel matrices [82]. For drug encapsulation, meanwhile, characteristics similar to those of the manually prepared hydrogels were observed. A peak at 231 ℃ (metformin's melting point) was not seen in these thermograms. This indicates that successful encapsulation of the drug was achieved.

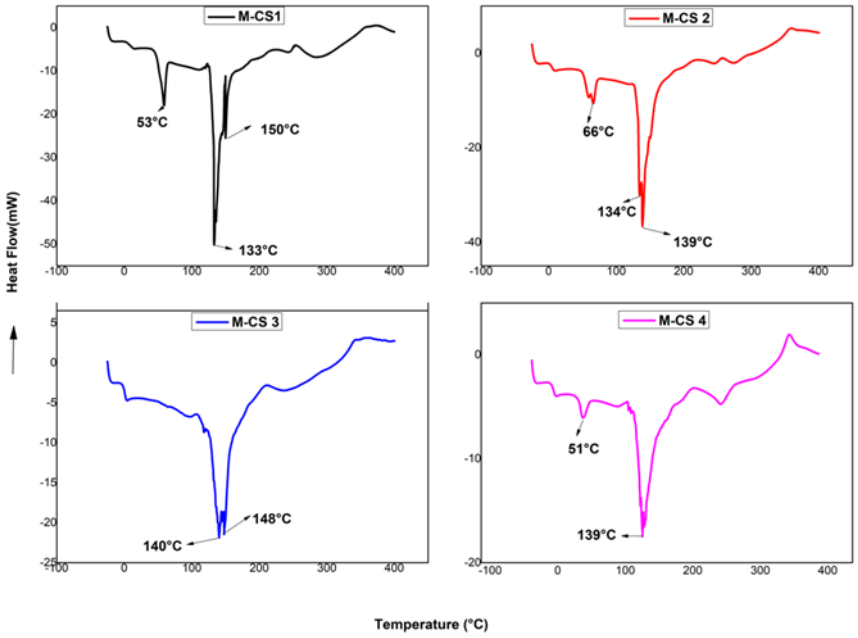

Figure 4.27: Chitosan powder (CS), microfluidically prepared CS/β-GP hydrogel (M-CS 1), microfluidically prepared CS/β-GP hydrogel with liposomal nanoparticles (M-CS 2), microfluidically prepared CS/β-GP hydrogel with metformin (M-CS 3), microfluidically prepared CS/β-GP hydrogel with metformin encapsulated nanoparticles (M-CS 4).

4.5. In vitro drug release study of produced nanocomposite hydrogels

In this study, 1% chitosan hydrogels were generated manually and via microfluidics and were physically dispersed with pure metformin and metformin encapsulated liposomal nanoparticles (1:1; w/w) after gelation. The dissolution of empty hydrogels (CS/β-GP) and combinations with the drug and freeze-dried drug-added liposomes was conducted at 25 ℃in 250 mL of PBS solution (pH 4.5). A UV-Vis device was used at 235 nm to obtain absorbance values (n=3). The drug release profiles of the hydrogels are shown in Figure 4.29. Before calculating % drug release, a calibration curve was generated for different concentrations of stock solution (metformin in PBS). Based on the calibration curve (Figure 4.28), the stock solution metformin in the solution of dissolution medium was generated, was used for the calculations of the amount of the drug released and percentage of drug released. Drug release graphs were then prepared to visualize drug release in the gels with and without encapsulation in nanoliposome vesicles.

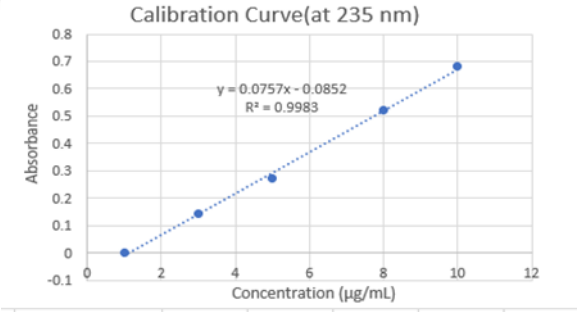

Figure 4.28: Calibration curve of standard solution of metformin HCl with different concentrations at pH 4.5.

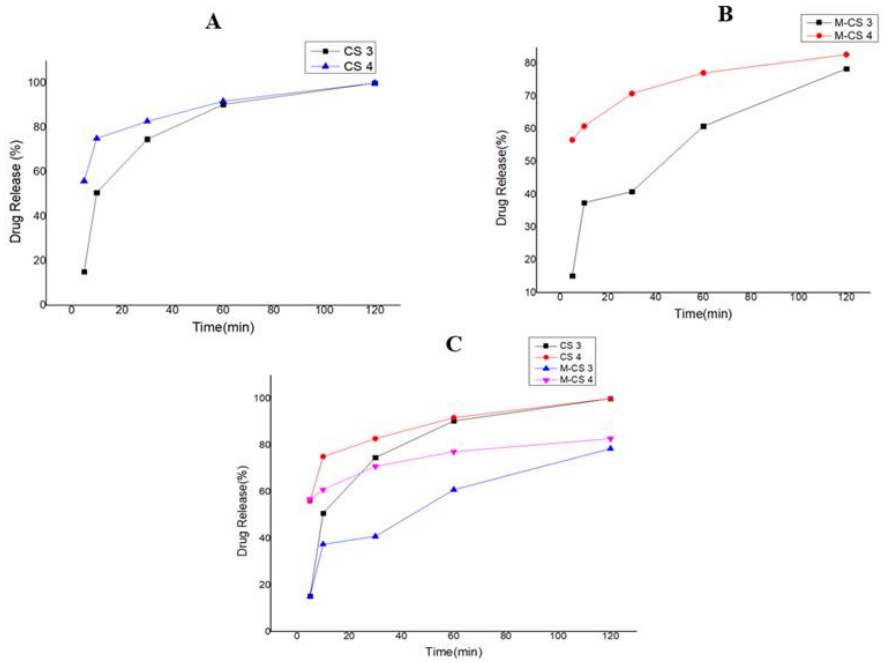

Figure 4.29: Drug release profiles of: A) manually generated 1% chitosan hydrogels with pure metformin (CS 3) and 1% chitosan incorporated with metformin encapsulated liposomal nanoparticles (1:1, w/w) after gelation (CS 4); B) microfluidically prepared 1% chitosan hydrogels with pure metformin (M-CS 3) and 1% chitosan hydrogel incorporated with freeze-dried metformin encapsulated liposomal nanoparticles (1:1, w/w) (M-CS 4) after gelation; C) 1% chitosan hydrogels that were produced by both methods (manual and microfluidics), manually prepared chitosan with pure metformin (CS 3), manually prepared gel incorporated with metformin encapsulated liposomal nanoparticles (CS 4), 1% hydrogel produced via microfluidics with pure metformin (M-CS-3), and 1% chitosan gel produced via microfluidics incorporated with metformin encapsulated liposomal nanoparticles (M-CS-4) (1:1, w/w), n=3.

Figure 4.29 demonstrates the percentage of drug release for both the manually and microfluidically prepared hydrogels with pure drug (metformin) and freeze-dried metformin-incorporated liposome vesicles. For the manually generated hydrogels, the dissolution profiles in PBS (pH 4.5) are provided in (Figure 4.29, A). The presented line graph shows different percentages of both hydrogels (with metformin and with

metformin encapsulated liposomal nanoparticles). Although different percentages of dissolution were obtained throughout the process, both hydrogels released the drug at the same rate, reaching a peak of 100% after 2 h. The hydrogel with incorporated nanoparticles together with metformin encapsulated liposomal nanoparticles had higher dissolution percentages compared to the hydrogel with the pure drug. Under the same dissolution conditions, the chitosan hydrogels produced microfluidically (Figure 4.29, B) also had different percentages of release. Similarly, to the manually produced hydrogels, the dissolution percentage peaked at 120 min. The chitosan hydrogel with metformin reached a peak of 60%, whereas the percentage of drug release for the hydrogel incorporated with lyophilized metformin encapsulated liposomal nanoparticles reached 82%. To summarize, the hydrogels incorporated with the nanoparticle form of metformin had higher levels of dissolution compared to the hydrogels (both manually and microfluidically produced) incorporated with pure metformin.

4.5.1. Results of kinetics for metformin release

After dissolution tests, drug release profiles were obtained. The dissolution profiles were investigated to observe the controlled drug release of the nanoparticle form of metformin encapsulated liposomal nanoparticles in hydrogel platforms, both manually and microfluidically (Figure 4.30). Three kinetic models were used to evaluate how the hydrogels might best fit the kinetic model for controlled drug release. In Figure 4.30, the percentage drug releases of metformin and metformin encapsulated liposomal nanoparticles are plotted according to different drug kinetic models to decide the most suitable model for the drug profile in the context of a controlled DDS based on R^2. The closer R^2 is to 1, the better the drug release profile fits the model. Therefore, the dissolution profiles of both pure metformin and metformin encapsulated liposomal nanoparticles in the hydrogels fit best within the framework of the Higuchi model (Table 4.3).

The values of each profile revealed an increase compared to the zero- and first-order release kinetic models. It was observed that the dissolution profile of the manually produced hydrogels was much higher than that of the microfluidically produced hydrogels. This may be due to losses in the course of the physical incorporation of the drug and nanoparticle metformin after the gelation process.

Overall, metformin encapsulated liposomal nanoparticles had a higher dissolution rate compared to metformin in hydrogel platforms.

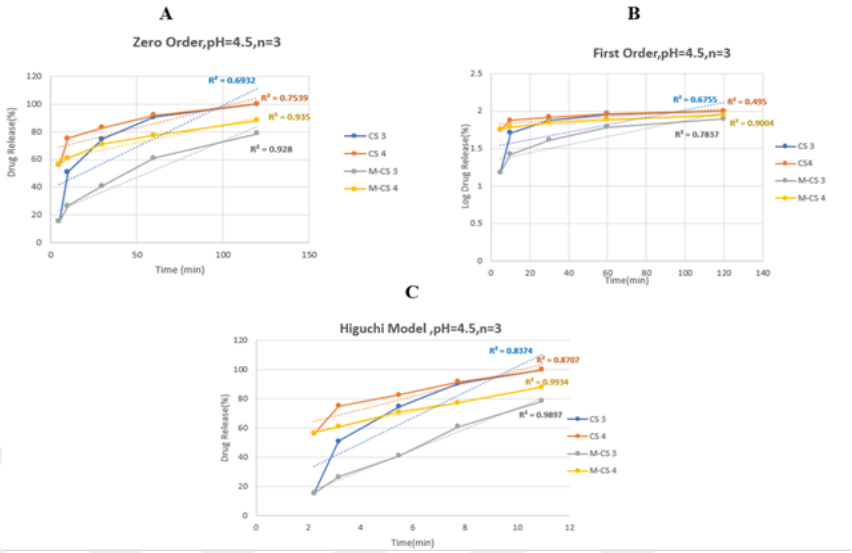

Figure 4.30: Kinetic models of controlled drug release of hydrogels (both manually and microfluidically prepared) with incorporation of metformin and metformin encapsulated liposomal nanoparticles: A) zero-order kinetics release profile of hydrogels, including manually prepared hydrogel incorporated with pure metformin (CS 3), manually prepared hydrogel incorporated with l metformin encapsulated liposomal nanoparticles (CS 4), microfluidically prepared hydrogel incorporated with metformin (M-CS 3), and microfluidically prepared hydrogel incorporated with metformin encapsulated liposomal nanoparticles (M-CS 4); B) first-order kinetics release; (C) Higuchi model release profile of hydrogels, n=3.

Table 4.3: Results from three kinetic models of metformin/ metformin encapsulated liposomal nanoparticles in different hydrogel platforms.

Time (60 min)	Zero-order	First-order	Higuchi model
Sample	R^2	R^2	R^2
CS 3	0.693	0.5	0.837
CS 4	0.754	0.676	0.871
M-CS 3	0.928	0.784	0.99
M-CS 4	0.935	0.91	0.933

4.5.2. Statistical analysis of metformin release

Dissolution data were collected after 60 and 120 min with three repeated measurements. The drug release of both pure metformin and metformin encapsulated liposomal nanoparticles was studied in two different hydrogel matrices with different production methods. After 60 min, it was seen that higher dissolution rates were associated with manually generated chitosan hydrogels (Figure 4.31). CS 3, which was physically incorporated with the pure drug, displayed 90% dissolution, and CS 4, the hydrogel incorporated with metformin encapsulated liposomal nanoparticles, had a dissolution value of 91%. On the other hand, microfluidically produced hydrogels exhibited much lower levels of dissolution at the end of 60 min. M-CS 3, the microbubble hydrogel incorporated with pure metformin, had a dissolution percentage of 61%, while M-CS 4, the microbubble hydrogel with metformin encapsulated liposomal nanoparticles, had a dissolution percentage of 77%. After 2 h, the dissolution profiles of CS 3 and CS 4 peaked at 100%. In contrast, the microbubble hydrogels demonstrated much lower dissolution rates for metformin with M-CS 3 at 79% and M-CS 4 at 83% (Figure 4.32).

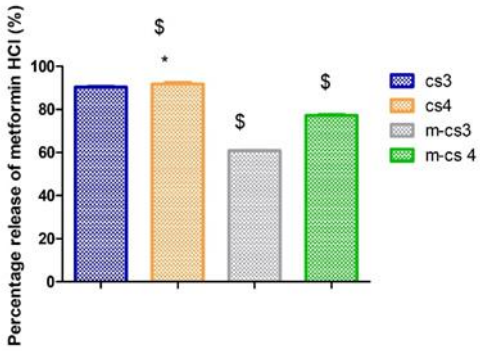

Figure 4.31: Dissolution percentages of metformin in different hydrogel platforms after 60 minutes (mean ± SD, n=3).

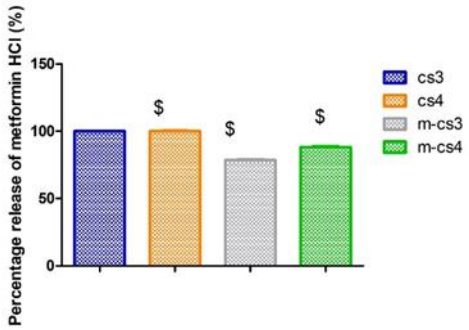

Figure 4.32: Dissolution percentages of metformin in hydrogels after 120 minutes (mean ± SD, n=3).

4.6. Characterization of drug-loaded liposome vesicles

4.6.1. Drug-loading efficiency of nanoliposomal particles

As seen in Table 4.4, the absorbance value of 2.5 mg of metformin in 10 mL of water was taken as the maximum value in terms of dissolution. According to the Beer-Lambert law, absorbance values must be below 1. Therefore, 2.5 mg of metformin in 10 mL of water had absorbance of 0.91 at 235 nm in the first trial, which was assumed to be a maximum absorbance value below 1. If such a value is evaluated as being higher than or equal to 1, more dilution steps must be applied. Therefore, 10 trials were conducted for both the pure drug and lyophilized drug-incorporated liposomes for precise calculations. In each trial, approximately 1 mL of sample solution was transferred to a quartz cuvette [69]. The average absorbance value of pure metformin was found to be 0.9152 (Table 4.4), which was assumed to correspond to 100% of the drug in water. The average absorbance value of met: lec 1:1 (w/w) was then calculated as 0.7258. If the absorbance at 0.9152 is assumed as 100% of the drug present in the dissolution medium, then 0.7258 will represent the 79% of the drug encapsulated in lyophilized liposomes. The encapsulation capacity of metformin in liposomes was found to be acceptable based on the data reported in the literature [20, 82].

Table 4.4: Absorbance values of pure metformin and met: lec 1:1 (w/w) after being dissolved in pure water.

Absorbance (235 nm)		
Trials	**met**	**met: lec**
1	0.91	0.726
2	0.907	0.733
3	0.921	0.738
4	0.917	0.726
5	0.917	0.724
6	0.91	0.719
7	0.914	0.719
8	0.921	0.724
9	0.921	0.724
10	0.914	0.725
Avg.	0.9152	0.7258

4.6.2. Liposomal nanoparticle sizes, zeta potentials, and polydispersity index (PDI)

According to the DLS data shown in Table 4.3, the average sizes of the drug-loaded and unloaded liposomes were 128.8 nm and 3.732 nm, respectively, while the diameters of the nanovesicles significantly increased from 3.732 nm to 128.8 nm due to the presence of metformin (Figure 4.33). The zeta potential of nano-sized drug-loaded vesicles were found to be -38, which is lower than negative values of - 40, (Figure 4.34) [83]. This indicates that the zeta potential of the vesicles was not within the range of agglomeration. Both blank and drug-incorporated liposomes showed high monodispersity; their PDI values were found to be below 0.4 (Table 4.5). The PDI values of nanoparticles play a key role in terms of stability [84].

Table 4.5: Vesicle characteristics with/without drug.

Name	Size, nm, mean	Zeta potential (mV)
Egg lecithin liposomes	3.732	-2.18
metformin encapsulated liposomal nanoparticles (1:1; w/w)	128.8	-38.1

Figure 4.33: Blank liposomal nanoparticles size distribution zeta potential.

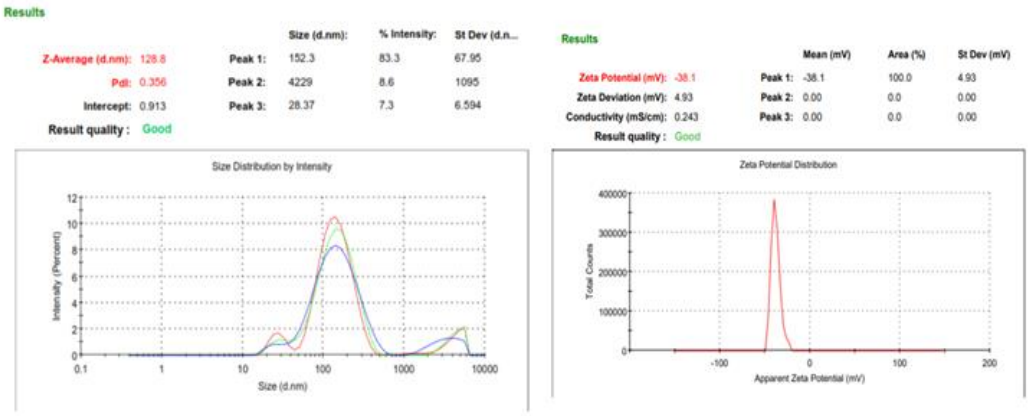

Figure 4.34: Metformin encapsulated nanoparticles, met: lec 1:1 (w/w) size distribution, and zeta potential.

5. DISCUSSION

This study was undertaken with the aim of preparing and evaluating nanoliposome drug-loaded vesicles and physically incorporating them with thermo-sensitive microfluidically prepared chitosan hydrogels for topical applications. The microfluidic approach was applied to evaluate controlled drug release with encapsulated liposomal nanoparticles. Accordingly, efforts were made to obtain nano-sized, drug-loaded liposomes with high monodispersity and high stability. With the help of these vesicles, as the subsequent aim of the research, the release of metformin after incorporation with microfluidically prepared hydrogels was expected to occur in a controlled fashion. The main aim in these efforts to develop a gel for vaginal application was to overcome the side effects of metformin, which are generally reported as gastrointestinal problems. Another reason for pursuing vaginal topical application was the absorption ability of the vagina. Chitosan was chosen for its high biocompatibility and mucoadhesive nature. Chitosan is a cationic polymer and vaginal mucin is negatively charged; this interaction of charges may accordingly allow easier drug targeting in the vaginal environment [45].

In line with the hypothesis, the results of this analysis demonstrate that nano-sized drug-loaded vesicles and nanosized monodispersed microbubbles were achieved (Chapters 4.3.1 and 4.6.2). In terms of drug release and drug-loading efficiency, dissolution tests were conducted. The drug release performances of metformin/ metformin encapsulated liposomal nanoparticles confirmed the controlled release into chitosan hydrogels at pH 4.5. Based on the considered mathematical models, having obtained Plateau-like drug release profiles (Figure 4.30), the dissolution profiles of the drug and its nanoparticle form under vaginal pH conditions demonstrated controlled drug release behaviour over a 2-h interval of time. The dissolution rates of metformin encapsulated liposomal nanoparticles for both manually and microfluidically generated nanocomposite hydrogels were much higher than those for the pure drug. This could be explained by egg lecithin having possibly increased the solubility of the metformin. It was also reported that metformin is a BCS type III drug and thus has low permeability [85]. Therefore, the dissolution rate was increased with the liposomal form of metformin, leading to elevated drug permeability of the metformin. Moreover, it was previously reported that pharmaceutical surfactants increase the drug permeability into cell membranes [86].

Thus, the nano-sized liposomal drugs increased not only the drug permeability but also the bioavailability of the drug.

In Chapter 4.5, the release profile of the microbubble hydrogels revealed an increase from 79% to 83%. The system that included both hydrophilic and hydrophobic structures had higher solubility. After 120 min of dissolution, maximum drug release was seen to have been achieved for both types of hydrogels (manually and microfluidically prepared). The dissolution rate of the microfluidically prepared hydrogels was much lower, however, than that of the manually produced hydrogels. The dissolution rates of microbubble hydrogels for M-CS 3 and M-CS 4 were 79% and 83%, respectively. In the literature, it was similarly reported that metformin dissolution was prolonged with microbubble hydrogel platforms [87]. Hence, the controlled drug delivery of metformin was pursued in the present research. With microbubble-controlled DDSs, that goal was achieved. Moreover, the drug-loading efficiency was found to be 79%. In other words, 79% of the drug was encapsulated in the lyophilized metformin encapsulated liposomal nanoparticles.

Encapsulation was also evaluated by FTIR and DSC analysis, as well as by SEM. There were no unexpected chemical reactions while adding the drug to the liposomes and incorporating them after gelation into the hydrogel platforms. According to the SEM images, the microbubbles of the CS/β-GP ionically crosslinked hydrogels (see Figure 4.20) had a homogeneous porous morphology. This was expected via microfluidics, where pore sizes are reduced compared to manually prepared samples. Optical microscopy illustrated the monodispersed chitosan microbubbles; monodispersity is a key factor affecting the homogeneity of pores in a hydrogel matrix. High homogeneity of hydrogels facilitates controlled drug release. However, the pore size distribution of the microfluidically produced hydrogels has pore PDI values higher than conventionally produced hydrogels (see Figure 4.21). This could be associated with the bubbling frequency of the microfluidics system, maybe the pressure applied in high amplitudes affected the bubble size distribution so that the bubbles were inconsistent with the changes in the applied pressure [79].

The research performed within the framework of this thesis differs from previous studies in the literature [41, 46, 73]. For example, Saini et al., 2016 evaluated the production methods for both hydrogels and drug-loaded liposomes. The probe sonication method was used for drug-loaded liposomal nanoparticles. Compared to

other means of producing nanoliposomes (e.g., thin film hydration or ether injection), probe sonication did not require toxic chemicals such as chloroform. The lyophilization process was then conducted; studies of liposome stability and dispersion into the hydrogel after gelation were pursued. A T-shaped microfluidic system was used to generate monodispersed microbubble hydrogels with monodispersed microbubbles of chitosan together with precise ionic gelation. Therefore, this study has provided a novel approach for producing composite hydrogel systems for vaginal drug delivery. Compared to the study conducted by Saini et al., 2016, the drug entrapment efficiency obtained in the present work was higher (79%). As a difference between these studies, in vitro drug release was monitored here for 2 h instead of 24 h. For controlled vaginal drug delivery, 24 h is generally considered to be a long time because the vagina cleans itself. Therefore, 2 h of controlled drug release with lower drug dosages is a more promising strategy for vaginal controlled DDSs. Hence, the research conducted here has yielded better results in terms of the potential of disease treatment via topical vaginal applications.

In conclusion, the nanocomposite hydrogel platforms produced here may be promising candidates for topical vaginal applications because of several unique features. Utilizing the microfluidics technique allowed for the creation of a slow-release DDS, and incorporating them with liposomal drug carriers enhanced the bioavailability of the drug. Reducing the dose of the drug with sonication and lyophilization also led the surface area of the drug to increase. Thus, all side effects and unwanted outcomes were avoided. These microbubble chitosan hydrogel platforms are suitable candidates for vaginal drug delivery with controlled release and lower numbers of dosages. Based on this study, future work may focus on in vivo drug release experiments, and changes in the formulations of both metformin encapsulated liposomal nanoparticles and the crosslinked chitosan hydrogel platforms can be evaluated in more detail.

Further research might also consider pre-formulations of nanoliposomes with a drug rather than a single ratio of 1:1 (w/w). Other drug: surfactant ratios such as 1:2 or 1:3 could be considered. In addition, crosslinking ratios and types could be changed. Regarding the concentration of the polymer, the polymer properties could be measured at different temperatures because the concentration, surface tension, and density are directly proportional to the size of the microbubbles. This would also help optimize the size distribution of the microbubbles. In vivo dissolution experiments

could furthermore be conducted to adjust the dosage reduction and drug release. Several dissolution experiments with different physiological pH values could be conducted to evaluate the dissolution and release rates of metformin HCl at different pH levels. Considering the production technique for the nanocomposite hydrogels, different junction types of microfluidic devices could be selected for the simultaneous production of liposomal drug-loaded carriers and hydrogel platforms.

REFERENCES

[1] Alhussain F., Alruthia Y., Al-Mandeel H., Bellahwal A., Alharbi F., Almogbel Y., Alharbi F.A., (2020), "Metformin improves the depression symptoms of women with polycystic ovary syndrome in a lifestyle modification program", Patient Preference and Adherence, 14, 737–746.

[2] Litvak J., Parekh N., Juul F., Deierlein A., (2020), "Food assistance programs and income are associated with the diet quality of grocery purchases for households consisting of women of reproductive age or young children", Preventive Medicine, 138 (December 2019), 106149.

[3] Iversen L., Fielding S., Lidegaard Ø., Mørch L. S., Skovlund C. W., Hannaford P. C., (2018), "Association between contemporary hormonal contraception and ovarian cancer in women of reproductive age in Denmark: Prospective, nationwide cohort study", BMJ (Online), 362, 1–9.

[4] Bednarska S., Siejka, A., (2017), "The pathogenesis and treatment of polycystic ovary syndrome: What's new?", Advances in Clinical and Experimental Medicine, 26(2), 359–367.

[5] Bailey C. J., (2017), "Metformin: historical overview", Diabetologia, 60(9), 1566–1576.

[6] Wang M., Duan, B., (2019), "Materials and their biomedical applications", Encyclopedia of Biomedical Engineering (Vol. 1–3), Elsevier Inc.

[7] MacLeod P. J., Hamer G. K., Lukose P., Georges M. K., (2019), "Functional Polymers: (H. Mazumder, Abu Jafafar Mohammad Sheardown & A. Al-Ahmed, Eds.)", Polymers and Polymeric composites: A Reference Series, Springer International Publishing.

[8] Zhang Y., Huang Y., (2021), "Rational Design of Smart Hydrogels for Biomedical Applications",. Frontiers in Chemistry, 8.

[9] Crocini C., Walker C. J., Anseth, K. S., Leinwand, L. A., (2020), "Three-dimensional encapsulation of adult mouse cardiomyocytes in hydrogels with tunable stiffness", Progress in Biophysics and Molecular Biology, 154, 71–79.

[10] Golafshan N., Rezahasani R., Tarkesh Esfahani M., Kharaziha M., Khorasani S. N., (2017), "Nanohybrid hydrogels of laponite: PVA-Alginate as a potential wound healing material", Carbohydrate Polymers, 176, 392–401.

[11] Adrian G., Mihai M., Vodnar D. C., (2019), "The Use of Chitosan, Alginate, and Pectin in the Biomedical and Food Sector-Biocompatibility, Bioadhesiveness, and Biodegradability", Polymers (Basel), 11(11), 1837.

[12] Sohrabi S., Kassir N., Keshavarz Moraveji M., (2020), "Droplet microfluidics: Fundamentals and its advanced applications", RSC Advances, 10(46).

[13] Daly A. C., Riley L., Segura, T., Burdick J. A., (2020), "Hydrogel microparticles for biomedical applications", Nature Reviews Materials, 5(1), 20–43.

[14] Yanar F., Mosayyebi A., Nastruzzi C., Carugo D., Zhang, X., (2020), "Continuous- flow production of liposomes with a millireactor under varying fluidic conditions", Pharmaceutics, 12(11), 1–21.

[15] Dimitriou P., Li, J. Tornillo, G., McCloy T., Barrow D., (2021), "Droplet Microfluidics for Tumor Drug- Related Studies and Programmable Artificial Cells", Global Challenges, 2000123, 2000123.

[16] Zhao Q., Cui H., Wang Y., Du, X., (2020), "Microfluidic Platforms toward Rational Material Fabrication for Biomedical Applications", Small, 16(9), 1–22.

[17] Ushikubo F. Y., Birribilli F. S., Oliveira D. R. B., Cunha R. L., (2014) ," Y- and T-junction microfluidic devices: effect of fluids and interface properties and operating conditions", Microfluidics and Nanofluidics, 17(4), 711–720.

[18] Kucuk I., Ahmad Z., Edirisinghe M., Orlu-Gul M., (2014), "Utilization of microfluidic V-junction device to prepare surface itraconazole adsorbed nanospheres", International Journal of Pharmaceutics, 472(1–2), 339–346.

[19] Mutlu B., Farhan M., Kucuk I., (2019), "T-shaped microfluidic junction processing of porous alginate-based films and their characteristics", Polymers, 11(9).

[20] Liu Y., Tottori N., Nisisako, T., (2019), "Microfluidic synthesis of highly spherical calcium alginate hydrogels based on external gelation using an emulsion reactant", Sensors and Actuators, B: Chemical, 283(September 2018), 802–809.

[21] Joshi S., Hussain M. T., Roces,C. B., Anderluzzi G., Kastner E., Salmaso S., Perrie Y., (2016), "Microfluidics based manufacture of liposomes simultaneously entrapping hydrophilic and lipophilic drugs", International Journal of Pharmaceutics, 514(1), 160–168.

[22] Sosnik A., Seremeta K., (2017), "Polymeric Hydrogels as Technology Platform for Drug Delivery Applications", Gels, 3(3), 25.

[23] Zahir-Jouzdani F., Wolf J. D., Atyabi, F., Bernkop-Schnürch, A., (2018), "In situ gelling and mucoadhesive polymers: why do they need each other ?", Expert Opinion on Drug Delivery, 15(10), 1007–1019.

[24] Cook M. T., Brown M. B., (2018), "Polymeric gels for intravaginal drug delivery", Journal of Controlled Release, 270, 145–157.

[25] Skiba M. A., Islam R. M., Bell R. J., Davis S. R., (2018), "Understanding variation in prevalence estimates of polycystic ovary syndrome: A systematic review and meta-analysis", Human Reproduction Update, 24(6), 694–709.

[26] Milman N., Taylor C. L., Merkel J., Brannon P. M., (2017), "Iron status in pregnant women and women of reproductive age in Europe", American Journal of Clinical Nutrition, 106, 1655S-1662S.

[27] Wolf W. M., Wattick R. A., Kinkade O. N., Olfert, M. D., (2018), "Geographical prevalence of polycystic ovary syndrome as determined by region and race/ethnicity", International Journal of Environmental Research and Public Health, 15(11), 1–13.

[28] Azziz R Carmina E., Chen Z., Dunaif A., Laven JS., Legro RS., Lizneva D., Natterson-Horowtiz B., Teede HJ., Y. B., (2016), "Polycystic Ovary Syndrome", Nat Rev Dis Primers, 11(2), 6057.

[29] Mukerjee N., (2020), "Polycystic Ovary Syndrome (PCOS) Symptoms Causes & Treatments - A Review", International Journal of Science and Research,

9(7).

[30] He Y., Lu Y., Zhu Q., Wang, Y., Lindheim S. R., Qi J., Sun Y., (2019), "Influence of metabolic syndrome on female fertility and in vitro fertilization outcomes in PCOS women", American Journal of Obstetrics and Gynecology, 221(2), 138.e1-138.e12.

[31] Macut D., Božić-Antić I., Bjekić-Macut J., Tziomalos K., (2017), "Management of endocrine disease: Polycystic ovary syndrome and nonalcoholic fatty liver disease", European Journal of Endocrinology, 177(3), R145–R158.

[32] Doretto L., Mari, F. C., Chaves, A. C., (2020), "Polycystic Ovary Syndrome and Psychotic Disorder", Frontiers in Psychiatry, 11(June), 1–6.

[33] Azziz R., Carmina E., Chen Z., Dunaif A., Laven J. S. E., Legro R. S., Yildiz B. O., (2016), "Polycystic ovary syndrome", Nature Reviews Disease Primers, 2.

[34] Escobar-Morreale H. F., (2018), "Polycystic ovary syndrome: Definition, aetiology, diagnosis and treatment", Nature Reviews Endocrinology, 14(5), 270–284.

[35] Teede H. J., Misso M. L., Costello M. F., Dokras A., Laven J., Moran L., Yildiz B. O., (2018), "Recommendations from the international evidence-based guideline for the assessment and management of polycystic ovary syndrome", Fertility and Sterility, 110(3), 364–379.

[36] Leyva-Gómez G., Piñón-Segundo E., Mendoza-Muñoz N., Zambrano-Zaragoza M. L., Mendoza-Elvira S., Quintanar-Guerrero D., (2018), "Approaches in polymeric nanoparticles for vaginal drug delivery: A review of the state of the art", International Journal of Molecular Sciences, 19(6), 1–19.

[37] Della Corte L., Foreste V., Barra F., Gustavino C., Alessandri F., Centurioni M. G., Giampaolino P.,(2020), "Current and experimental drug therapy for the treatment of polycystic ovarian syndrome", Expert Opinion on Investigational Drugs, 29(8), 819–830.

[38] Morley L. C., Tang T., Yasmin E., Norman R. J., Balen A. H., (2017), "Insulin-sensitising drugs (metformin, rosiglitazone, pioglitazone, D-chiro-inositol) for women with polycystic ovary syndrome, oligo amenorrhoea and subfertility", Cochrane Database of Systematic Reviews, 2017(11).

[39] Shpakov A. O., (2021)," Improvement effect of Metformin on female and male reproduction in endocrine pathologies and its mechanisms", Pharmaceuticals, 14(1), 1–45.

[40] Sanjay S. T., Zhou, W., Dou, M. Tavakoli, H. Ma, L., Xu F., Li X. J., (2018), "Recent advances of controlled drug delivery using microfluidic platforms", Advanced Drug Delivery Reviews, 128, 3–28.

[41] Nys G., Fillet, M., (2018), "Microfluidics contribution to pharmaceutical sciences: From drug discovery to post marketing product management", Journal of Pharmaceutical and Biomedical Analysis, 159, 348–362.

[42] Saini N., Sodhi R. K., Bajaj L., Pandey R. S., Jain, U. K., Katare O. P., Madan, J., (2016), "Intravaginal administration of metformin hydrochloride loaded cationic niosomes amalgamated with thermosensitive gel for the treatment of polycystic ovary syndrome: In vitro and in vivo studies", Colloids and Surfaces B: Biointerfaces, 144, 161–169.

[43] Mansuri S., Kesharwani P., Jain K., Tekade R. K., Jain N. K., (2016), "Mucoadhesion: A promising approach in drug delivery system", Reactive and Functional Polymers, 100, 151–172.

[44] Rohani Shirvan A., Bashari A., Hemmatinejad N., (2019), "New insight into the fabrication of smart mucoadhesive buccal patches as a novel controlled-drug delivery system", European Polymer Journal, 119(July), 541–550.

[45] Rahmanian-Devin P., Baradaran Rahimi V., Askari V. R., (2021), "Thermosensitive Chitosan- β -Glycerophosphate Hydrogels as Targeted Drug Delivery Systems: An Overview on Preparation and Their Applications", Advances in Pharmacological and Pharmaceutical Sciences, 2021.

[46] Ways T. M. M., Lau W. M., Khutoryanskiy V. V., (2018), "Chitosan and its derivatives for application in mucoadhesive drug delivery systems", Polymers , 10(3).

[47] Manconi M., Nácher A., Merino V., Merino-Sanjuan M., Manca M. L., Mura C., Diez-Sales,O., (2013), "Improving Oral Bioavailability and Pharmacokinetics of Liposomal Metformin by Glycerolphosphate-Chitosan Microcomplexation", AAPS PharmSciTech, 14(2), 485-496.

[48] Park W., Shin H., Choi B., Rhim W. K., Na K., Keun Han D., (2020), "Advanced hybrid nanomaterials for biomedical applications", Progress in Materials Science, 114(May), 100686.

[49] Lavrador P., Esteves M. R., Gaspar V. M., Mano J. F., (2021), "Stimuli-Responsive Nanocomposite Hydrogels for Biomedical Applications", Advanced Functional Materials, 31(8), 1–30.

[50] Alvarez-Lorenzo C., Grinberg V. Y., Burova, T. V., Concheiro A., (2020), "Stimuli-sensitive cross-linked hydrogels as drug delivery systems: Impact of the drug on the responsiveness", International Journal of Pharmaceutics, 579(February), 119157.

[51] Bhattarai N., Gunn J., Zhang M., (2010), "Chitosan-based hydrogels for controlled, localized drug delivery", Advanced Drug Delivery Reviews, 62(1), 83–99.

[52] López-Noriega A., Hastings C. L., Ozbakir B., O'Donnell, K. E., O'Brien F. J., Storm G., Ruiz-Hernández E., (2014), "Hyperthermia-Induced Drug Delivery from Thermosensitive Liposomes Encapsulated in an Injectable Hydrogel for Local Chemotherapy", Advanced Healthcare Materials, 3(6), 854–859.

[53] Tan C., Wang J., Sun B., (2021), "Biopolymer-liposome hybrid systems for controlled delivery of bioactive compounds: Recent advances", Biotechnology Advances, 48.

[54] Gholamali I., Yadollahi M., (2021), "Bio-nanocomposite Polymer Hydrogels Containing Nanoparticles for Drug Delivery: a Review", Regenerative Engineering and Translational Medicine, 7, 129-146.

[55] Wang C., Piao J., Li Y., Tian X., Dong Y., Liu, D., (2020), "Construction of Liposomes Mimicking Cell Membrane Structure through Frame-Guided Assembly", Angewandte Chemie - International Edition, 59(35), 15176–15180.

[56] Parashar M., Shukla V. K., Singh R., (2020), "Metal oxides nanoparticles via sol–gel method: a review on synthesis, characterization and applications", Journal of Materials Science: Materials in Electronics, 31(5), 3729–3749.

[57] Hamdallah S. I., Zoqlam R., Erfle P., Blyth M., Alkilany A. M., Dietzel, A., Qi, S., (2020), "Microfluidics for pharmaceutical nanoparticle fabrication: The truth and the myth", International Journal of Pharmaceutics, 584(January).

[58] Niculescu, A.-G., Chircov, C., Bîrcă, A. C., Grumezescu, A. M., De Morais, P. C., (2021), "Nanomaterials Synthesis through Microfluidic Methods: An Updated Overview ", Nanomaterials(Basel), 11(4), 864.

[59] Kucuk I., (2016), "Microfluidic Engineered Polymer Nanovehicles for Drug Delivery" - UCL Discovery. UCL (University College London). Retrieved March 27, 2022, from https://discovery.ucl.ac.uk/id/eprint/1475164/

[60] Ma Q., Cao J., Gao Y., Han S., Liang Y., Zhang T., Sun Y., (2020), "Microfluidic-mediated nano-drug delivery systems: From fundamentals to fabrication for advanced therapeutic applications", Nanoscale, 12(29), 15512–15527.

[61] Radwan S. E. S., Sokar M. S., Abdelmonsif D. A., El-Kamel A. H., (2017), "Mucopenetrating nanoparticles for enhancement of oral bioavailability of furosemide: In vitro and in vivo evaluation/sub-acute toxicity study", International Journal of Pharmaceutics, 526(1–2), 366–379.

[62] Toprakcioglu Z., Kumar Challa P., Morse D. B., Knowles T., (2020), "Attoliter protein nanogels from droplet nanofluidics for intracellular delivery", 6(6), 1-9.

[63] Watanabe T., Motohiro I., Ono T., (2019), "Microfluidic Formation of Hydrogel Microcapsules with a Single Aqueous Core by Spontaneous Cross-Linking in Aqueous Two-Phase System Droplets", Langmuir, 35(6), 2358–2367.

[64] Paarakh M. P., Jose P. A. N. I., Setty C. M., Peter G. V., (2019), "Release Kinetics – Concepts and Applications", International Journal of Pharmacy Research & Technology, 8(1), 12–20.

[65] Dash S., Murthy P. N., Nath L., Chowdhury P., (2010), "Kinetic modeling on drug release from controlled drug delivery systems", Acta Poloniae

Pharmaceutica - Drug Research, 67(3), 217–223.

[66] Yuksel N., Kanik A. E., Baykara T., (2000), "Comparison of in vitro dissolution profiles by ANOVA-based, model-dependent and -independent methods", International Journal of Pharmaceutics, 209(1–2), 57–67.

[67] Dange Y. D., Honmane S. M., Bhinge S. D., Salunkhe V. R., Jadge D. R., (2017), "Development and validation of uv-spectrophotometric method for estimation of metformin in bulk and tablet dosage form", Indian Journal of Pharmaceutical Education and Research, 51(4), S754–S760.

[68] Adhikari L., Jagadev S., Sahoo S., Murthy P. N., Mishra U. S., (2012), "Devlopement and validation of UV-visible spectrophotometric method for simultaneous determination of pioglitazone hydrochloride, metformin hydrochloride and glipizide in its bulk and pharmaceutical dosage form (Tablet)", International Journal of ChemTech Research, 4(2), 625–630.

[69] Pharma D., Ambadekar S., Keni S. S., Nikam D. B., (2017), "Fast and Simple Method for Assay Determination of Metformin and Glyburide from Combination Tablet Dosage form by UV Spectrophotometer", Der Pharma Chemica, 9(21), 70–78.

[70] Raza A., Khan H. N., Alom N. J., Haq U., (2019), "To Determine the Concentration Of Cobalt (II) In The Cobalt (II) Nitrate Hexahydarate Solution by UV-Visible Spectroscopy", IOSR Journal of Applied Chemistry (IOSR- JAC, 12(December), 22–27.

[71] Panda, B. P., Krishnamoorthy, R., Shivashekaregowda, N. K. H., Patnaik, S., (2018), "Influence of poloxamer 188 on design and development of second generation PLGA nanocrystals of metformin hydrochloride", Nano Biomedicine and Engineering, 10(4), 334–343.

[72] Kim D. W., Park J. B, (2015), "Development and pharmaceutical approach for sustained-released metformin succinate tablets", Journal of Drug Delivery Science and Technology, 30, 90–99.

[73] Latif M. H., Alsouz M. A. K., Taher M. B., (2014), "Quantification of the components of the Iraqi Chicken wet egg yolk, and characterization of Lecithin", Chemistry and Materials Research, 6(6), 42–48.

[74] Zhou F., Xu T., Zhao Y., Song H., Zhang L., Wu X., Lu B., (2018), "Chitosan-coated liposomes as delivery systems for improving the stability and oral bioavailability of acteoside", Food Hydrocolloids, 83, 17–24.

[75] De Souza Costa E., Pereira M. M., Mansur H. S., (2009), "Properties and biocompatibility of chitosan films modified by blending with PVA and chemically crosslinked", Journal of Materials Science: Materials in Medicine, 20(2), 553–561.

[76] Mansur H. S. de S. Costa Jr., E., Mansur A. A. P., Barbosa-Stancioli E. F., (2009), "Cytocompatibility evaluation in cell-culture systems of chemically crosslinked chitosan/PVA hydrogels", Materials Science and Engineering C, 29(5), 1574–1583.

[77] Pieklarz K., Galita G., Tylman M., Maniukiewicz W., Kucharska E., Majsterek I.,Modrzejewska Z., (2021), "Physico-chemical properties and biocompatibility of thermosensitive chitosan lactate and chitosan chloride hydrogels developed for tissue engineering application", Journal of Functional Biomaterials, 12(2).

[78] Skwarczynska A., Kaminska, M., Owczarz P., Bartoszek N., Walkowiak B., Modrzejewska Z., (2018), "The structural (FTIR, XRD, and XPS) and biological studies of thermosensitive chitosan chloride gels with β-glycerophosphate disodium", Journal of Applied Polymer Science, 135(27), 1–8.

[79] Parhizkar M., Stride E., Edirisinghe M., (2014), "Preparation of monodisperse microbubbles using an integrated embedded capillary T-junction with electrohydrodynamic focusing", Lab on a Chip, 14(14), 2437–2446.

[80] Andrieux S., Drenckhan W., Stubenrauch C., (2018), "Generation of Solid Foams with Controlled Polydispersity Using Microfluidics", Langmuir, 34(4), 1581–1590.

[81] Parhizkar M., (2014), "Preparation of monodisperse microbubbles in a capillary embedded T-Junction device and the influence of process control parameters on bubble size and stability", Lab on a chip, 14(14), 2437-2446.

[82] Bischoff R., CrayS.E., (1999), "Polysiloxanes in macromolecular architecture", Progress in Polymer Science (Oxford), 24(2), 185–219.

[83] Honary S., Zahir F., (2013), "Effect of zeta potential on the properties of nano-drug delivery systems - A review (Part 1)", Tropical Journal of Pharmaceutical Research, 12(2), 255–264.

[84] Bhattacharjee S., (2016), "DLS and zeta potential - What they are and what they are not?", Journal of Controlled Release, 235, 337–351.

[85] Cheng C. L., Yu L. X., Lee H. L., Yang C. Y., Lue C. S., Chou C. H., (2004), "Biowaiver extension potential to BCS Class III high solubility-low permeability drugs: Bridging evidence for metformin immediate-release tablet", European Journal of Pharmaceutical Sciences, 22(4), 297–304.

[86] Gaynanova G., Vasileva L., Kashapov R., Kuznetsova D., Kushnazarova R., Tyryshkina A., Sinyashin O., (2021), "Self-assembling drug formulations with tunable permeability and biodegradability", Molecules, 26(22).

[87] Wu X., He C., Wu Y., Chen X., (2016), "Synergistic therapeutic effects of Schiff's base cross-linked injectable hydrogels for local co-delivery of metformin and 5-fluorouracil in a mouse colon carcinoma model", Biomaterials, 75, 148–162.

CURRICULUM VITAE

Melda Elmas graduated from the Department of Chemical Engineering, in the Faculty of Engineering, at Yeditepe University with a B.Sc. degree in 2018. Following her graduation, she successfully completed several master's degree courses at Acıbadem University, with an emphasis on Medical Engineering. As of spring 2019, she started her master's degree in Nanoscience and Nanoengineering at Gebze Technical University Institute of Nanotechnology.